Nonlinear model predictive control of a continuous slab reheating furnace

authored by **A. Steinboeck, D. Wild, and A. Kugi**

and published in *Control Engineering Practice*.

Contact:

Automation and Control Institute (ACIN)
Vienna University of Technology
Gusshausstrasse 27-29/E376
1040 Vienna, Austria

Internet: www.acin.tuwien.ac.at
E-mail: office@acin.tuwien.ac.at
Phone: +43 1 58801 37601
Fax: +43 1 58801 37699

Nonlinear model predictive control of a continuous slab reheating furnace☆

A. Steinboeck[a,*], D. Wild[b], A. Kugi[a]

[a] *Automation and Control Institute, Vienna University of Technology, Gußhausstraße 27–29, 1040 Wien, Austria*
[b] *Aktiengesellschaft der Dillinger Hüttenwerke, Werkstrasse 1, 66763 Dillingen/Saar, Germany*

Abstract

A nonlinear model predictive controller is designed for a continuous reheating furnace for steel slabs. Based on a first-principles mathematical model, the controller defines local furnace temperatures so that the slabs reach their desired final temperatures. The controller is suitable for non-steady-state operating situations and reaching user-defined desired slab temperature profiles. In the control algorithm, a nonlinear unconstrained dynamic optimization problem is solved by the quasi-Newton method. The design of the controller exploits the fact that the considered slab reheating furnace is a continuous production process. Long-term measurement results from an industrial application of the controller demonstrate its reliability and accuracy.

Keywords: Nonlinear model predictive control, Continuous slab reheating furnace, Nonlinear switched MIMO system, Unconstrained optimization, Quasi-Newton method

1. Introduction

1.1. Furnace control problem

Slab furnaces are used for heat treatment of steel slabs or for reheating them before they undergo some hot working process. Continuous slab furnaces, like the one considered in this paper (cf. Fig. 1), operate in a continuous manner in the sense that slabs are charged into the furnace at one side, are moved through the furnace while being heated, and are discharged at the opposite side. Despite the name continuous slab furnace, the slab movement itself may be discontinuous. In the furnace considered in this work (cf. Fig. 1), an electromechanical charging ram pushes the row of slabs through the furnace. The furnace is used in a heavy-plate rolling mill, can process slabs with a maximum thickness of 0.45 m, and has a maximum throughput rate of steel slabs of 280 t/h. The heat is supplied by gas- and oil-fired burners, which have a total capacity of 185 MW.

Temperature control of slab furnaces is of crucial importance to safety, product quality, the achievable throughput rate, and the energy consumption. However, temperature control is a challenging task for the following reasons: The slab temperatures, i. e., the most relevant process variables, cannot be measured. The thermal behavior of the system is rather slow because both the slabs and the furnace enclosure are characterized by high thermal inertia. The observed time constants are of the same order of magnitude as the reheating times of slabs. A slab reheating furnace is essentially a multi-input multi-output (MIMO) distributed parameter system with nonlinear physical interactions like thermal radiation. The heat flows supplied by the burners serve as control variables. Clearly, they are bounded above and below. The slab temperature depends significantly on the feed rate of the slabs, which is generally governed by up- or downstream process steps. The range of products (dimensions, steel grade, target temperature, reheating time) is continuously increasing and changes of product types are frequent. In some cases, the furnace may even contain one-off products. Therefore, the heating process is characterized by non-steady-state operation.

Due to the large time constants, pure feedback control may fail to meet the stringent accuracy requirements in terms of slab temperatures. Therefore, a feedforward or predictive control approach seems best suited for this task. The known future production plan including all relevant parameters of the slabs should be utilized in the control law as early as possible. In the current paper, the suitability of model predictive control for the considered furnace control problem is explored.

1.2. Existing solutions

Model predictive control (cf. Camacho and Bordons, 2004; Findeisen et al., 2007; Grüne and Pannek, 2011) is a versatile optimization-based control method, which has significantly benefited from soaring computing power during the last few years. While the application of model predictive control to continuous furnace processes (cf. Stadler et al., 2011), especially slab furnace control problems (cf. Nederkoorn et al., 2011), is a rather recent research topic,

☆Handling editor: Ian K. Craig.
*Corresponding author. *Tel.:* +43 1 58801 376264, *fax:* +43 1 58801 9376264.
Email addresses: andreas.steinboeck@tuwien.ac.at (A. Steinboeck), daniel.wild@dillinger.biz (D. Wild), kugi@acin.tuwien.ac.at (A. Kugi)

Post-print version of the article: A. Steinboeck, D. Wild, and A. Kugi, "Nonlinear model predictive control of a continuous slab reheating furnace", *Control Engineering Practice*, vol. 21, no. 4, pp. 495–508, 2013. DOI: 10.1016/j.conengprac.2012.11.012

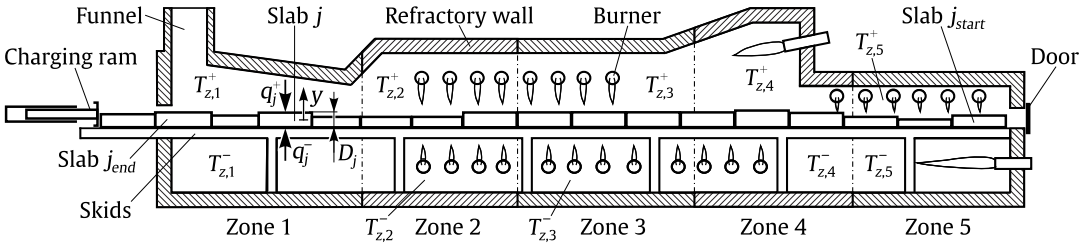

Figure 1: Pusher-type slab reheating furnace (not to scale).

optimization methods have been used in this field already in the 1970s (Pike and Citron, 1970; Wörk, 1971). For brevity, the following brief literature review is restricted to model-based dynamic optimization applied to continuous reheating furnaces for steel slabs.

Two categories of optimal furnace controllers may be distinguished: First, the heat input through the burners—or their fuel flow rates—can be directly optimized. This approach requires a detailed mathematical model which must capture the nexus between the heat supplied by the burners and the furnace temperatures. Second, the optimization algorithm may generate optimum furnace temperatures, which are then used in subordinate control loops for the burners.

The work of Pike and Citron (1970) belongs to the first category. They used both static and dynamic optimization for offline preplanning of fuel flow rates of a continuous slab reheating furnace. In their model, the slabs are represented by mean temperatures only. The same is true for the models presented by Balbis et al. (2008) and Fujii et al. (2010), who optimized fuel flow rates and the furnace production schedule at the same time. Fujii et al. (2010) used mixed integer linear programming in a linear model predictive controller. Balbis et al. (2008) optimized steady-state furnace temperatures based on a nonlinear model and a linear cost function. In a subordinate control loop, a linear model predictive controller regulates the fuel supplies and the movement of the slabs.

The real-time control strategy developed by Yoshitani et al. (1994) belongs also to the first category. They solved the heat conduction problem in the slabs by means of the Galerkin method and formulated a nonlinear optimization problem for generating reference trajectories of slab temperatures. Finally, the fuel flow rates are obtained by a linear model predictive control algorithm.

Using feedback linearization, a linear model of the gas temperatures in a continuous billet furnace was derived by Choi et al. (2001). Based on this model, they developed a linear model predictive controller for the fuel supplies to the burners. Ko et al. (2000) used the same furnace model as Choi et al. (2001) and proposed a system identification algorithm and a linear model predictive controller for the fuel flow rates.

The nonlinear model predictive controller developed by Nederkoorn et al. (2011) governs local furnace temperatures and the throughput rate of slabs. Thus the method belongs to the second category of slab furnace controllers. The model used in the controller assumes a homogeneous slab temperature, which is justifiable for the rather thin products reheated in the concerned furnace. Nederkoorn et al. (2011) reported that their controller can save up to 10 % of the primary energy consumption compared to manually controlling the furnace.

The predictive control scheme proposed by Icev et al. (2004) belongs also to the second category. A linear system model, which was identified from step response measurements, serves as constraint of a quadratic optimization problem. A real-time generalized predictive controller (cf. Camacho and Bordons, 2004) yields optimal local furnace temperatures.

The real-time algorithms developed in (Marino et al., 2004; Steinboeck et al., 2011c; Sugiyama et al., 1999) use simple predictive optimization routines for trajectory planning and furnace control. At each sampling point, a minimization problem is solved for finding optimum setpoint values of local furnace temperatures. The quadratic cost functions depend mainly on the deviations between the expected and the desired heat inputs into the slabs. Marino et al. (2004) and Sugiyama et al. (1999) compute the desired heat inputs based on target temperatures of the slabs at the end of each furnace section. Steinboeck et al. (2011c) used a simple state feedback controller for this purpose. These algorithms lack optimization horizons, which limits their performance compared to model predictive control.

1.3. Motivation and objectives

Most existing furnace control systems that use dynamic optimization are based on linear system models or the assumption of homogeneous slab temperatures or both. Notwithstanding that these modeling approaches simplify the design of the controller, they may limit the scope and the accuracy of the obtained controllers.

Continuous slab reheating furnaces are complex dynamical systems, which vary significantly with regards to design and product properties. Hardly any industrial slab furnace is a duplicate, implying that the control solutions proposed in the literature naturally cannot cater for the great variety of custom-made and individually operated reheating furnaces. Each slab furnace design requires a

Post-print version of the article: A. Steinboeck, D. Wild, and A. Kugi, "Nonlinear model predictive control of a continuous slab reheating furnace", *Control Engineering Practice*, vol. 21, no. 4, pp. 495–508, 2013. DOI: 10.1016/j.conengprac.2012.11.012
The content of this post-print version is identical to the published paper but without the publisher's final layout or copy editing.

tailored control system and provides ample scope for research and development.

All these facts induced the motivation to develop a new furnace temperature control strategy that harnesses the power of nonlinear model predictive control (Findeisen et al., 2007; Grüne and Pannek, 2011) for non-steady-state furnace operation. The current work aims at:

- Accurate control of slab temperatures
- Maximum throughput of reheated material
- Optimum product quality and minimum loss of material through scale formation

Control design for slab reheating furnaces has to respect several constrains:

- Bounds on the temperatures of the furnace interior and the furnace walls (damage and wear prevention)
- Safety regulations
- Limitations of the control inputs
- Metallurgical requirements for the slab reheating process (Chen, 2009)
- Process times prescribed by supervisory plant controllers that coordinate all production steps

Moreover, there are some recent trends in furnace operation, which call for advanced control strategies. Though the approach pursued in this paper will not cater for all these trends, some pertinent drivers of improved control design are:

- Increasing diversity of products and materials, e. g., increasing slab thickness and layered slabs
- Reduction of energy consumption and CO_2 emissions
- Hot charging (Chen, 2009)
- Furnace control based on a unified mathematical model that covers all operating situations
- Automatic handling of start up, shut down, and (unforeseen) production halts (Nederkoorn et al., 2011)
- Recuperative or regenerative burners (Wuenning, 2007)

Given the many aspects and requirements of slab furnace operation, the control of these systems is challenging for theorists and practitioners alike. This paper is addressed to both of them. Engineers and operators should find the fundamental ingredients for developing a nonlinear model predictive controller for their specific system. Moreover, theorists may find in this paper an industrial application of nonlinear model predictive control that is beyond the laboratory level.

1.4. Structure

The paper is organized as follows: Based on first principles, a mathematical model of the considered slab reheating furnace is developed in Section 2. In Section 3, the cascade structure of a furnace control system is explained and the control objectives are formally specified. A model predictive controller is developed in Section 4 and tested in a simulated example problem in Section 5. In Section 6, long-term results from an industrial application of the controller are presented.

2. Mathematical model

For control design, a model that was originally published by Steinboeck et al. (2010) is used. In the current paper, a discrete-time version of the model is described and convection is considered as an additional mode of heat transfer (cf. Steinboeck et al., 2011b). The essential features of the models presented by Steinboeck et al. (2011b, 2010) are briefly repeated to ensure a self-contained presentation and a solid basis for control design in subsequent sections.

The controller is developed and tested in a simulation environment where the real furnace is emulated by the elaborate model of Wild et al. (2009). This model is based on heat and mass balances for discrete volume elements of the furnace interior. Heat is exchanged between the burners, the bulk flow of flue gas, the refractory furnace walls, and the slabs. The 1-dimensional temperature profile inside the slabs is computed by means of the finite difference method with radiation boundary conditions.

The low-dimensional and computationally undemanding model used in the current paper is simpler than the model of Wild et al. (2009) and was tailor-made for model-based control design. The inputs of the model are the local furnace temperatures, which are continuously measured in the real plant. On a standard personal computer (2.4 GHz dual core, 2 GB RAM), the model requires less than 1 s CPU time for simulating one full week of furnace operation. This is three orders of magnitudes faster than the model of Wild et al. (2009) and thus suitable for repeated evaluation in some optimization-based control algorithm.

2.1. Notation and geometry

Consider the furnace shown in Fig. 1. Each slab is identified by a constant index $j \in \mathbb{N}$ and the slabs $j \in \{j_{start}, \dots, j_{end}\}$ are currently inside the furnace. They are sorted in ascending order. The abbreviation $\bar{J} = j_{start}, \dots, j_{end}$ is used, i. e., $j = \bar{J}$ is tantamount to $j = j_{start}, \dots, j_{end}$. Let the slab j be reheated during the interval $[t_{j,0}, t_{j,1}]$. At the charging and discharging times $t_{j,0}$ and $t_{j,1}$, the indices j_{start} and j_{end} are appropriately incremented. All times when slabs change their position shall be summarized in the sequence (t_K^s) with $K \in \mathbb{N}$.

As indicated in Fig. 1, D_j is the thickness of the slab j along the direction y. Moreover, the abbreviations $\Omega = (-D_j/2, D_j/2)$ and $\bar{\Omega} = [-D_j/2, D_j/2]$ are used. The local coordinate $y \in \bar{\Omega}$ is individually defined for each slab such that $y = 0$ holds at the slab mid-plane.

2.2. Heat conduction equation

For computing the temperature profile $T_j(y,t)$ of the slab j along the direction y (vertical direction in Fig. 1), consider the 1-dimensional heat conduction equation

$$\rho_j c_j(T_j)\frac{\partial T_j}{\partial t} = \frac{\partial}{\partial y}\Big(\lambda_j(T_j)\frac{\partial T_j}{\partial y}\Big) \quad y \in \Omega,\, t > t_{j,0} \qquad (1)$$

with Neumann boundary conditions $q_j^{\mp}(t) = \mp\lambda_j(T_j)\partial T_j/\partial y|_{y=\mp D_j/2}$ (cf. Fig. 1) and the initial

Post-print version of the article: A. Steinboeck, D. Wild, and A. Kugi, "Nonlinear model predictive control of a continuous slab reheating furnace", *Control Engineering Practice*, vol. 21, no. 4, pp. 495–508, 2013. DOI: 10.1016/j.conengprac.2012.11.012
The content of this post-print version is identical to the published paper but without the publisher's final layout or copy editing.

condition $T_j(y, t_{j,0}) = T_{j,0}(y)$. Henceforth, variables belonging to the bottom or top half of the furnace shall be labeled with the superscripts $^-$ or $^+$, respectively. The mass density ρ_j is considered to be constant. The specific heat capacity c_j and the thermal conductivity λ_j, however, depend on the local temperature T_j (BISRA, 1953).

The Galerkin weighted residual method with orthogonal trial functions $h_{j,1}(y) = 1$, $h_{j,2}(y) = 2y/D_j$, and $h_{j,3}(y) = (2y/D_j)^2 - 1/3$ is used for solving the problem (1). The approximate temperature field thus takes the form $T_j(y,t) = [h_{j,1}(y), h_{j,2}(y), h_{j,3}(y)]\boldsymbol{x}_j(t)$, where the vector $\boldsymbol{x}_j(t)$ contains the Galerkin states $x_{j,1}(t)$, $x_{j,2}(t)$, and $x_{j,3}(t)$. Their time evolution follows the system

$$\dot{\boldsymbol{x}}_j(t) = \boldsymbol{a}_j \boldsymbol{x}_j(t) + \boldsymbol{b}_j^- q_j^-(t) + \boldsymbol{b}_j^+ q_j^+(t) \qquad t > t_{j,0} \tag{2}$$

with

$$\boldsymbol{a}_j = -\frac{12\bar{\lambda}_j}{\rho_j \bar{c}_j D_j^2} \begin{bmatrix} 0 & 0 & 0 \\ 0 & 1 & 0 \\ 0 & 0 & 5 \end{bmatrix}, \qquad \boldsymbol{b}_j^\mp = \frac{1}{\rho_j \bar{c}_j D_j} \begin{bmatrix} 1 \\ \mp 3 \\ 15/2 \end{bmatrix}.$$

The initial state corresponding to $T_{j,0}(y)$ is defined as $\boldsymbol{x}_j(t_{j,0}) = \boldsymbol{x}_{j,0}$ and the variables

$$\bar{\lambda}_j = \frac{1}{2x_{j,2}} \int_{\bar{\Omega}} \lambda_j \frac{\partial T_j}{\partial y} \,\mathrm{d}y, \qquad \bar{c}_j = \frac{1}{x_{j,1} D_j} \int_{\bar{\Omega}} c_j T_j \,\mathrm{d}y$$

represent weighted mean values (cf. Steinboeck et al., 2010). If λ_j and c_j were constant, (2) would be linear.

The chosen parameterization of the temperature profile facilitates a straightforward physical interpretation: The Galerkin coefficient $x_{j,1}(t)$ is the mean temperature of the slab, $x_{j,2}(t)$ defines the asymmetric inhomogeneity of $T_j(y,t)$, and $x_{j,3}(t)$ represents the transient, symmetric inhomogeneity. This conception will be helpful when formulating an optimization-based control law. Moreover, this parameterization yields a sufficiently accurate approximation of the slab surface temperature, i. e., $T_j(\mp D_j/2, t) = [1, \mp 1, 2/3]\boldsymbol{x}_j(t)$. It will be used for evaluating boundary conditions in Section 2.5.

2.3. Switched system

The states and surface heat fluxes of all slabs $j \in J$ are summarized in the vectors $\boldsymbol{X}(t) = [\boldsymbol{x}_j(t)]_{j=\bar{J}}$ and $\boldsymbol{q}^\mp(t) = [q_j^\mp(t)]_{j=\bar{J}}$ so that the state-space system reads as

$$\dot{\boldsymbol{X}}(t) = \boldsymbol{A}\boldsymbol{X}(t) + \boldsymbol{B}^- \boldsymbol{q}^-(t) + \boldsymbol{B}^+ \boldsymbol{q}^+(t) \tag{3}$$

with the sparse matrices $\boldsymbol{A} = \left[\delta_{i,j}\boldsymbol{a}_j\right]_{i=\bar{J},j=\bar{J}}$ and $\boldsymbol{B}^\mp = \left[\delta_{i,j}\boldsymbol{b}_j^\mp\right]_{i=\bar{J},j=\bar{J}}$, the initial state $\boldsymbol{X}_0 = \boldsymbol{X}(t_0) = [\boldsymbol{x}_j(t_0)]_{j=\bar{J}}$, and the Kronecker delta $\delta_{i,j}$. The dimensions and components of $\boldsymbol{X}(t)$, $\boldsymbol{A}$, $\boldsymbol{B}^\mp$, and $\boldsymbol{q}^\mp(t)$ may change at the times t_K^s. Therefore, (3) constitutes a switched system, which is taken into account when discretizing the system in the next step.

2.4. Discrete-time system

As suggested by Steinboeck et al. (2010), a generally non-uniform time grid $t_k, t_{k+1}, \ldots$ with $k \in \mathbb{N}$ and the sampling period $\Delta t_k = t_{k+1} - t_k$ is used. The switching times t_K^s serve as seed nodes and additional grid points are generated in the intervals (t_K^s, t_{K+1}^s) upon demand. For discretizing the model, the material parameters c_j and λ_j are assumed to change their values only at sampling points t_k and that the heat fluxes $\boldsymbol{q}^\mp(t)$ are piecewise linear, i. e.,

$$\boldsymbol{q}^\mp(t) = \boldsymbol{q}_{k,+}^\mp \frac{t_{k+1} - t}{\Delta t_k} + \boldsymbol{q}_{k+1,-}^\mp \frac{t - t_k}{\Delta t_k} \qquad \forall\, t \in [t_k, t_{k+1})$$

with the nodal values $\boldsymbol{q}_{k,+}^\mp = \lim_{\tau \to 0^+} \boldsymbol{q}^\mp(t_k + \tau)$ and $\boldsymbol{q}_{k,-}^\mp = \lim_{\tau \to 0^-} \boldsymbol{q}^\mp(t_k + \tau)$. By means of these reasonable approximations, the discrete-time system reads as

$$\begin{aligned} \boldsymbol{X}_{k+1} = \boldsymbol{A}_k \boldsymbol{X}_k &+ \boldsymbol{B}_{k,+}^- \boldsymbol{q}_{k,+}^- + \boldsymbol{B}_{k,+}^+ \boldsymbol{q}_{k,+}^+ \\ &+ \boldsymbol{B}_{k+1,-}^- \boldsymbol{q}_{k+1,-}^- + \boldsymbol{B}_{k+1,-}^+ \boldsymbol{q}_{k+1,-}^+ \qquad k \geq 0 \end{aligned} \tag{4}$$

with the initial state $\boldsymbol{X}_0 = [\boldsymbol{x}_{j,0}]_{j=\bar{J}}$ and the sparse matrices

$$\begin{aligned} \boldsymbol{A}_k &= \exp((t_{k+1} - t_k)\boldsymbol{A}) \\ \boldsymbol{B}_{k,+}^\mp &= \boldsymbol{B}^\mp \int_{t_k}^{t_{k+1}} \exp((t_{k+1} - \tau)\boldsymbol{A}) \frac{t_{k+1} - \tau}{\Delta t_k} \mathrm{d}\tau \\ \boldsymbol{B}_{k+1,-}^\mp &= \boldsymbol{B}^\mp \int_{t_k}^{t_{k+1}} \exp((t_{k+1} - \tau)\boldsymbol{A}) \frac{\tau - t_k}{\Delta t_k} \mathrm{d}\tau. \end{aligned}$$

2.5. Nonlinear boundary conditions

Note that (4) is a decoupled system, suggesting that it could be evaluated individually for each slab. However, the heat fluxes $\boldsymbol{q}^\mp(t)$ at the slab surfaces depend on the heat transfer mechanisms inside the furnace and couple the temperature evolution of all slabs. The radiative and convective heat exchange is considered, which can be included in the form (cf. Steinboeck et al., 2011b)

$$\boldsymbol{q}^\mp(t) = \boldsymbol{q}_R^\mp(t) + \boldsymbol{q}_C^\mp(t). \tag{5a}$$

As indicated in Fig. 1, the furnace is partitioned into $N_z = 5$ volume zones below and $N_z = 5$ zones above the slabs. Let $T_{z,i}^\mp(t)$ with $i \in \{1, \ldots, N_z\}$ be a representative combination of the local gas temperature and the local surface temperatures of the furnace walls. These temperatures are summarized in the vectors $\boldsymbol{T}_z^\mp(t) = [T_{z,i}^\mp(t)]_{i=1,\ldots,N_z}$ and serve as model inputs.

Based on the net radiation method (Modest, 2003; Siegel and Howell, 2002) with the assumption of gray-body radiation, constant emissivities, and negligible radiative interaction with the flue gas, the radiative heat flux densities $\boldsymbol{q}_R^\mp(t)$ into the slab surfaces can be computed as

$$\boldsymbol{q}_R^\mp(t) = \boldsymbol{P}_s^\mp(t)(\boldsymbol{M}^\mp \boldsymbol{X}(t))^4 + \boldsymbol{P}_z^\mp(t)(\boldsymbol{T}_z^\mp(t))^4, \tag{5b}$$

where $\boldsymbol{M}^\mp = [\delta_{i,j}[1, \mp 1, 2/3]]_{i=\bar{J},j=\bar{J}}$ maps $\boldsymbol{X}(t)$ to the slab surface temperatures. The matrices $\boldsymbol{P}_s^\mp(t)$ and $\boldsymbol{P}_z^\mp(t)$ are

Post-print version of the article: A. Steinboeck, D. Wild, and A. Kugi, "Nonlinear model predictive control of a continuous slab reheating furnace", *Control Engineering Practice*, vol. 21, no. 4, pp. 495–508, 2013. DOI: 10.1016/j.conengprac.2012.11.012

constant within each interval $[t_k, t_{k+1})$, i. e., they are piecewise constant. They depend on the radiative properties and the geometry of the furnace interior, which generally changes at the times t_K^s due to slab movements. The properties of $\boldsymbol{P}_s^{\mp}(t)$ and $\boldsymbol{P}_z^{\mp}(t)$ are discussed in more detail in (Steinboeck et al., 2010). The computation of $\boldsymbol{P}_s^{\mp}(t)$ and $\boldsymbol{P}_z^{\mp}(t)$ involves higher integrals but can be simplified if the geometry is approximated by a 2-dimensional scenario (cf. Steinboeck et al., 2010). The fourth power in (5b) is a heritage of the Stefan-Boltzmann law of radiation (Modest, 2003). The operation is to be applied individually to each component of the respective vector.

Due to the high temperatures in the furnace, thermal radiation is the dominant mode of heat exchange (Ko et al., 2000; Nederkoorn et al., 2011; Wild et al., 2009). Convective heat transfer (Kays et al., 2005), which can be considered as the second most important heat transfer effect in a slab furnace (Han et al., 2010; Kim et al., 2000), is modeled in the conventional way by the term (cf. Steinboeck et al., 2011b)

$$\boldsymbol{q}_C^{\mp}(t) = \boldsymbol{\alpha}(\boldsymbol{N}\boldsymbol{T}_z^{\mp}(t) - \boldsymbol{M}^{\mp}\boldsymbol{X}(t)). \tag{5c}$$

Here, $\boldsymbol{\alpha}$ is a diagonal matrix containing convective heat transfer coefficients for all slabs inside the furnace (cf. Kays et al., 2005). $\boldsymbol{N}$ is a sparse matrix that maps the zone temperatures to all slabs that are currently in the respective zone. Interpolation is used for slabs that reside at the interface between two furnace zones. The sums of column elements of $\boldsymbol{N}$ are 1. Convective heat exchange is a linear phenomenon and proportional to the local temperature difference only. Radiative heat transfer, on the contrary, involves a fourth-power nonlinearity and depends on the temperature of all participating volumes and surfaces, not just the local ones.

The nonlinear mapping (5) captures the most relevant modes of heat exchange inside the furnace. They are the essential reason for the dynamic interaction between the slabs and also between the slabs and their environment. Therefore, the model represents a MIMO system. Relation (5) is evaluated at each sampling point t_k—strictly speaking, the left- and right-hand-side limits are computed—to obtain $\boldsymbol{q}_{k,+}^{\mp}$ and $\boldsymbol{q}_{k+1,-}^{\mp}$, which are required in (4).

2.6. Parameterizing and assembling the model

In principle, all parameters used in the model are known from design drawings or material handbooks. Hence, the model could be used as is (cf. Steinboeck et al., 2010). More accurate results are, however, achieved if parameters are tuned. The emissivities occurring in $\boldsymbol{P}_s^{\mp}(t)$ and $\boldsymbol{P}_z^{\mp}(t)$ and the convection coefficients in $\boldsymbol{\alpha}$ are good choices for parameter identification. For this purpose, a test slab equipped with thermocouples and a water-cooled data recorder is reheated in the furnace. Then, the simulated temperature trajectory of the test slab is fitted to the measured curve by parameter tuning.

The discrete-time state-space model (4) with (5) being evaluated at the sampling points is rewritten as

$$\boldsymbol{0} = \boldsymbol{F}_k(\boldsymbol{X}_{k+1}, \boldsymbol{X}_k, \boldsymbol{u}_{k+1}, \boldsymbol{u}_k) \qquad k \geq 0 \tag{6}$$

with the initial state $\boldsymbol{X}_0$ and the input $\boldsymbol{u}_k = [(\boldsymbol{T}_z^-(t_k))^T, (\boldsymbol{T}_z^+(t_k))^T]^T$. Because of the boundary conditions, the model is implicit. It contains states of all slabs that are currently inside the furnace. States enter and exit the model synchronous with slab charging and discharging events.

Finally, the model is recast into a format that is compatible with standard notation of state-space systems. Consider that the furnace should be analyzed during a certain time interval $[t_{k_0}, t_{k_1}]$ and let $\boldsymbol{z}_k = [\ldots, \boldsymbol{x}_{j_{start}-1,k}^T, \boldsymbol{X}_k^T, \boldsymbol{x}_{j_{end}+1,k}^T, \ldots]^T$ contain the states of all slabs that are in the furnace sometimes during this interval. For slabs outside the furnace ($j \notin J$), the trivial assumption of a steady state is imposed, i. e., $\boldsymbol{x}_{j,k+1} = \boldsymbol{x}_{j,k}\ \forall\, j \notin J$. The complete state-space model thus follows in the form

$$\begin{aligned} \boldsymbol{0} &= \boldsymbol{f}_k(\boldsymbol{z}_{k+1}, \boldsymbol{z}_k, \boldsymbol{u}_{k+1}, \boldsymbol{u}_k) \\ &= \begin{bmatrix} \boldsymbol{F}_k(\boldsymbol{X}_{k+1}, \boldsymbol{X}_k, \boldsymbol{u}_{k+1}, \boldsymbol{u}_k) \\ \boldsymbol{x}_{j,k+1} - \boldsymbol{x}_{j,k}\ \forall\, j \notin J \end{bmatrix} \quad k = k_0, \ldots, k_1 - 1 \end{aligned} \tag{7}$$

with the appropriately assembled initial state $\boldsymbol{z}_{k_0} = \boldsymbol{z}_0$. This system can be easily integrated, e. g., by means of the Newton-Raphson method. The fact that it is an implicit model is beneficial for numerical stability. The system serves as a basis for developing a model predictive controller in Section 4.

3. Furnace temperature control system

The primary physical inputs of the continuous slab reheating furnace are the path-time diagrams of the slabs, their properties (geometry, steel grade, initial temperature), and the fuel and air supplies to the burners. In the current section, it is briefly explained why defining all these inputs by a single control algorithm would be inordinately complex and how cascade control reduces this complexity. Fig. 2 shows the hierarchical control structure proposed for the considered furnace.

The principal control objective is that the slabs accurately reach their desired final temperature within the available reheating time. This objective is complemented

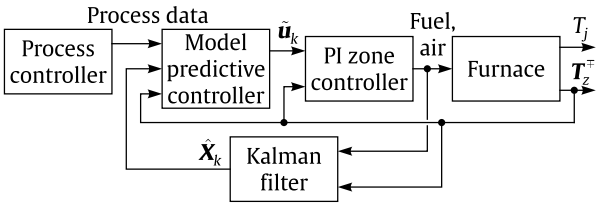

Figure 2: Cascade control structure.

Post-print version of the article: A. Steinboeck, D. Wild, and A. Kugi, "Nonlinear model predictive control of a continuous slab reheating furnace", *Control Engineering Practice*, vol. 21, no. 4, pp. 495–508, 2013. DOI: 10.1016/j.conengprac.2012.11.012
The content of this post-print version is identical to the published paper but without the publisher's final layout or copy editing.

by safety requirements, limitations of the control inputs, various metallurgical requirements as regards slab temperature development, and the desire for optimum product quality and maximum output. How do these multiple control objectives and constraints materialize in the choice of the primary control inputs? This challenging question is greatly simplified if the control task is split into several hierarchical layers.

Another reason why a hierarchical control structure, especially cascade control, caters well for continuous slab reheating furnaces is the coincidence of very different response times in these systems. Typical time constants range from fractions of a second for burner valves up to several hours associated with the thermal inertia of furnace brickwork. Indeed, cascade control is quite commonly used for such furnaces, e. g., by Balbis et al. (2008); Icev et al. (2004); Ko et al. (2000); Marino et al. (2004); Nederkoorn et al. (2011); and Wang et al. (2003, 2004).

3.1. Three hierarchical control layers

Fig. 2 indicates three layers of the hierarchical control system. At the topmost level, a process controller schedules all production steps of the rolling mill including the reheating procedure. The process controller defines the sequence of slabs, their reheating times, their target temperatures, and metallurgical constraints on their temperatures. These variables, which are referred to as process data, are summarized in Table 1. Many of them are chosen depending on the subsequent rolling step. The discharging time $t_{j,1}$, which is also chosen by the process controller, directly influences the throughput rate. Maximizing the throughput is thus a control objective associated with the topmost layer; the second control layer has no influence on the furnace speed.

In the second control layer, a model predictive controller selects reference values $\tilde{\boldsymbol{u}}_k$ for the furnace zone temperatures so that the slabs are reheated as desired. This model predictive controller is the centerpiece of this paper. The task of this controller is described at the end of this section and in more detail in Section 4.4. Alternatively, open-loop control (cf. Steinboeck et al., 2011a,c) or two-degrees-of-freedom control with a Lyapunov-based feedback law (cf. Steinboeck et al., 2011d) could be used. Steinboeck et al. (2011c) developed an open-loop ad-hoc iterative planning algorithm for the furnace zone temperatures. A similar open-loop planning problem was solved by Steinboeck et al. (2011a) using dynamic optimization based on a continuous-time model.

The slab temperatures, which are required as initial states of the model predictive controller, i. e., as feedback, cannot be measured in the real system. Even radiation pyrometry does not achieve sufficient accuracy because of the rough conditions in the furnace interior and uncertain radiation properties of the oxidized surfaces. Therefore, the slab temperatures are estimated using an extended Kalman filter developed by Wild (2010); Wild et al. (2007).

Variable	Description
$t_{j,0}$	Charging time
$t_{j,1}$	Discharging time
$\boldsymbol{x}_{j,0}$	Temperature state at $t_{j,0}$
$\tilde{\boldsymbol{x}}_{j,end}$	Desired final temperature state (at $t_{j,1}$)
$T_{j,abs,max}$ ...	Upper bound on slab temperature
$T_{j,hom}$	Minimum temperature during soaking period
$t_{k_{j,hom}}$	Beginning of soaking period
$T_{j,end,max}$ ...	Upper bound on final slab temperature profile
$T_{j,end,min}$ ...	Lower bound on final slab temperature profile
ρ_j	Mass density
$c_j(T_j)$	Specific heat capacity
$\lambda_j(T_j)$	Thermal conductivity
D_j	Thickness of the slab
w_j	Weighting factor reflecting the economic value of the slab

Table 1: Some parameters of the slab j specified by the process controller.

In the third layer, decentralized single-input single-output (SISO) controllers regulate the fuel and air supplies to the burners. Typically, PI- or PID-control is used at this level (cf. Icev et al., 2004; Nederkoorn et al., 2011). The PI controllers implemented in the furnace under consideration use the local furnace zone temperatures, which are measured by thermocouples, as feedback. Moreover, the measured zone temperatures serve as initial values in the model predictive controller. For designing this controller, $\tilde{\boldsymbol{u}}_k = \boldsymbol{u}_k = [(\boldsymbol{T}_z^-(t_k))^T, (\boldsymbol{T}_z^+(t_k))^T]^T$ is assumed, i. e., the inner control loop is considered ideal.

3.2. Control task

Starting with the slab temperature, a formal description of the control objectives and constraints is given. For convenience, these constraints are formulated for the discrete-time domain only. Consider that the slab j is inside the furnace during the sampling points $k_{j,0}, \ldots, k_{j,1}$, that means $t_{j,0} = t_{k_{j,0}}$ and $t_{j,1} = t_{k_{j,1}}$.

Fig. 3 shows constraints relevant for the temperature trajectory of slab j. To avoid creep or damage by over-

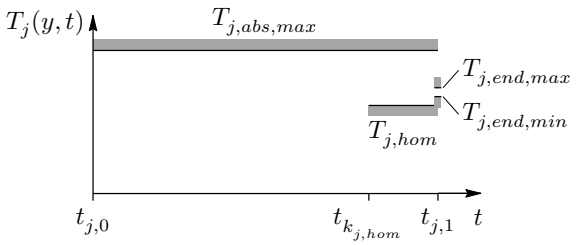

Figure 3: Constraints on slab temperature trajectory.

Post-print version of the article: A. Steinboeck, D. Wild, and A. Kugi, "Nonlinear model predictive control of a continuous slab reheating furnace", *Control Engineering Practice*, vol. 21, no. 4, pp. 495–508, 2013. DOI: 10.1016/j.conengprac.2012.11.012
The content of this post-print version is identical to the published paper but without the publisher's final layout or copy editing.

heating, the slab temperature is constrained by

$$T_j(y,t_k) \le T_{j,abs,max} \qquad y \in \bar{\Omega},\, k = k_{j,0},\ldots,k_{j,1}. \tag{8a}$$

Moreover, the slab temperature should obey

$$T_{j,hom} \le T_j(y,t_k) \qquad y \in \bar{\Omega},\, k = k_{j,hom},\ldots,k_{j,1} \tag{8b}$$

with $k_{j,0} \ll k_{j,hom} < k_{j,1}$. The interval $[t_{k_{j,hom}}, t_{j,1}]$ is referred to as soaking period. The constraint (8b) ensures that metallurgical phase change and temperature equalization can take place. When the slab j is finally discharged from the furnace, i. e., at the time $t_{j,1}$, it should have the desired final temperature state $\tilde{\boldsymbol{x}}_{j,end}$. Moreover, its final temperature profile is constrained by

$$T_{j,end,min} \le T_j(y,t_{j,1}) \le T_{j,end,max} \qquad y \in \bar{\Omega}. \tag{8c}$$

At first glance, the definition of both $\tilde{\boldsymbol{x}}_{j,end}$ and the allowed interval $[T_{j,end,min}, T_{j,end,max}]$ seems redundant. However, Section 6 will reveal that the limits $T_{j,end,min}$ and $T_{j,end,max}$ provide useful guidance for the controller if—for whatever reason—the desired state $\tilde{\boldsymbol{x}}_{j,end}$ cannot be reached. Further constraints, for instance, on the temperature asymmetry or inhomogeneity can be readily devised upon demand. In the current paper, the set of parameters given in Table 1 is used.

The furnace zone temperatures, i. e., the control inputs, are constrained in terms of both their absolute value and their slopes. Hence,

$$\underline{\boldsymbol{u}}_k \le \boldsymbol{u}_k \le \overline{\boldsymbol{u}}_k \qquad \forall\, k \tag{9a}$$

$$\underline{\dot{\boldsymbol{u}}}_k \le \frac{\boldsymbol{u}_k - \boldsymbol{u}_{k-1}}{\Delta t_{k-1}} \le \overline{\dot{\boldsymbol{u}}}_k \qquad \forall\, k, \tag{9b}$$

must be satisfied in the discrete-time domain. Here, the inequality signs are applied to corresponding components of the respective vectors. Note that $\underline{\boldsymbol{u}}_k$, $\overline{\boldsymbol{u}}_k$, $\underline{\dot{\boldsymbol{u}}}_k$, and $\overline{\dot{\boldsymbol{u}}}_k$ are generally independent. These constraints reflect that the furnace zone temperatures cannot change at arbitrary rates, e. g., due to limited burner capacity, the absence of cooling devices, and the risk of damaging the furnace walls. As long as $\tilde{\boldsymbol{u}}_k$ satisfies (9), the assumption $\tilde{\boldsymbol{u}}_k = \boldsymbol{u}_k$ seems justified.

The control objectives and constraints stated in this section correspond to those given in Section 1.3. Accurate control of the slab temperatures is the main objective and is directly related to the objective of optimum product quality and minimum loss of material through scale formation. Though the objective of maximum throughput of reheated material is associated with the topmost control level, the model predictive controller can help to improve the throughput rate by accurate slab temperature control and by fully utilizing the available reheating power of the furnace.

4. Model predictive controller

This section is devoted to the development of a nonlinear model predictive controller (cf. Findeisen et al., 2007; Grüne and Pannek, 2011) for a discrete-time system where state variables enter and leave the system in the course of time. It will be explored how this special model structure of a continuous production process complicates or eases the control problem. Finally, the control method is applied to the furnace control problem and augmented by an on-line adaptation strategy of the constraints.

The fundamental idea of model predictive control is that a finite-time dynamic optimization problem is recurrently solved based on a sufficiently accurate dynamic model. The current system state, which serves as feedback, enters the initial state of the optimization problem at the beginning of every optimization horizon. The following sections concentrate on the formulation and solution of the dynamic optimization problem.

Proving closed-loop stability of nonlinear model predictive control schemes is a rather challenging task, especially for high-dimensional, time-varying, switched systems like the one considered in this paper. Some results on the stability of nonlinear model predictive controllers have been published, for instance, in (Giselsson, 2010; Graichen and Kugi, 2010; Grüne, 2009; Grüne and Pannek, 2011; Pannek and Worthmann, 2011; Reble and Allgöwer, 2012). Many assumptions used in these works are not satisfied by the considered system, e. g., a constant number of states, absence of disturbances and model uncertainties, a steady-state operating point that is to be stabilized, knowledge of a suitable Lyapunov function, the existence of a terminal set or useful terminal equality constraints, or the exact solution of the underlying optimization problem. In view of these difficulties, a rigorous proof of closed-loop stability is a rather formidable task and thus beyond the scope of this paper.

From a practical point of view, the absence of a stability proof is acceptable. Steinboeck et al. (2010) proved that the open-loop controlled system is uniformly stable. Moreover, it is input-to-state stable, which is conforming to the second law of thermodynamics. Operation of the closed-loop controlled furnace system is thus safe as long as the inputs $\boldsymbol{u}_k$ are bounded—a requirement that is satisfied in this paper. The feedback controller just has to avoid the destabilization of an essentially good-natured plant.

4.1. Constrained optimization problem

For the finite optimization horizon $(t_{k_0}, t_{k_1}]$, consider the constrained nonlinear programming problem

$$\underset{\substack{\boldsymbol{u}_k \in \mathbb{R}^n \\ k = \bar{K}}}{\text{minimize}} \quad \sum_{k=\bar{K}} l_k(\boldsymbol{z}_k, \boldsymbol{u}_k) \tag{10a}$$

$$\text{subject to} \quad \boldsymbol{0} = \boldsymbol{f}_{k-1}(\boldsymbol{z}_k, \boldsymbol{z}_{k-1}, \boldsymbol{u}_k, \boldsymbol{u}_{k-1}), \quad k = \bar{K} \tag{10b}$$

$$\boldsymbol{z}_{k_0} = \boldsymbol{z}_0,\ \boldsymbol{u}_{k_0} = \boldsymbol{u}_0 \tag{10c}$$

$$\underline{\boldsymbol{u}}_k \le \boldsymbol{u}_k \le \overline{\boldsymbol{u}}_k, \qquad k = \bar{K} \tag{10d}$$

$$\underline{\dot{\boldsymbol{u}}}_k \le \frac{\boldsymbol{u}_k - \boldsymbol{u}_{k-1}}{\Delta t_{k-1}} \le \overline{\dot{\boldsymbol{u}}}_k, \qquad k = \bar{K} \tag{10e}$$

$$\boldsymbol{c}_k(\boldsymbol{z}_k) \le \boldsymbol{0}, \qquad k = \bar{K} \tag{10f}$$

Post-print version of the article: A. Steinboeck, D. Wild, and A. Kugi, "Nonlinear model predictive control of a continuous slab reheating furnace", *Control Engineering Practice*, vol. 21, no. 4, pp. 495–508, 2013. DOI: 10.1016/j.conengprac.2012.11.012
The content of this post-print version is identical to the published paper but without the publisher's final layout or copy editing.

with the abbreviation $\bar{K} = k_0 + 1, \ldots, k_1$ and the given initial values $\boldsymbol{z}_{k_0}$ and $\boldsymbol{u}_{k_0}$. The optimization problem (10) has $(k_1 - k_0)n$ optimization variables, where n is the number of controllable inputs.

The cost function l_k is to be chosen depending on the respective control objectives. Terminal costs can be included in l_{k_1}. Constraints on the system states $\boldsymbol{z}_k$ are captured by the function $\boldsymbol{c}_k$. Let l_k, $\boldsymbol{f}_k$, and $\boldsymbol{c}_k$ be continuous in their respective arguments. For the time being, $\boldsymbol{z}_k$, $\boldsymbol{f}_k$, and $\boldsymbol{c}_k$ are supposed to have a fixed dimension. Later, these vectors will be dynamically truncated to make use of the special switching structure of the system.

Without further assumptions, it is generally not sure whether a solution of (10) does exist and whether it is unique (cf. Keerthi and Gilbert, 1985, for a similar infinite-horizon problem). Apart from the switching character of the nonlinear system, the main challenges are the inequality constraints (10d), (10e), and (10f). These delicate issues are evaded by transforming (10) into an unconstrained representation. The approximation error entailed by this step is perfectly acceptable for the system considered in this paper. However, the following transformation is clearly not a panacea for any inequality constraint of a dynamic programming problem.

4.2. Conversion to an unconstrained optimization problem

In lieu of the box constraints (10d), the nonlinear map

$$\boldsymbol{u}_k = \boldsymbol{\varphi}_k(\boldsymbol{v}_k) = \frac{\overline{\boldsymbol{u}}_k + \underline{\boldsymbol{u}}_k}{2} + \frac{\overline{\boldsymbol{u}}_k - \underline{\boldsymbol{u}}_k}{2} \tanh\left(\frac{2\boldsymbol{v}_k}{\overline{\boldsymbol{u}}_k - \underline{\boldsymbol{u}}_k}\right) \quad (11)$$

is used with a new unconstrained input $\boldsymbol{v}_k$. Here, the mathematical operations are meant to be individually applied to the respective vector element. The sigmoid saturation function (11) (cf. Fig. 4 for a scalar illustration) ensures exact compliance with the original constraint (10d).

As shown by Graichen and Petit (2008), the formulation (11) has a significant drawback: It may cause singular arcs during those time intervals where the original constraint would be active, i. e., where at least one element of $\boldsymbol{v}_k$ approaches infinity. Graichen and Petit (2008) circumvented this problem by adding the positive definite term $1/2\varepsilon \boldsymbol{v}_k^T \boldsymbol{v}_k$ to the cost function l_k. Here, $\varepsilon > 0$ is a small penalty value. It can be shown that this formulation is comparable to using interior barrier functions and that it would yield exactly the same results as the original box constraints if $\varepsilon \to 0$ (Graichen and Petit, 2009).

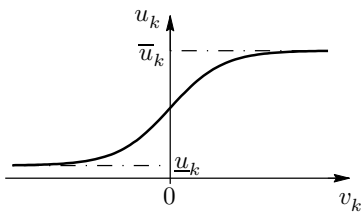

Figure 4: Saturation function for implementing box constraints (shown for a scalar input only).

Instead of the remaining inequality constraints (10e) and (10f), the exterior penalty terms

$$l_k^{\dot{u}}(\boldsymbol{u}_k, \boldsymbol{u}_{k-1}) = \eta \big\| \max(\boldsymbol{0}, \boldsymbol{u}_{k-1} - \boldsymbol{u}_k + \Delta t_{k-1}\underline{\dot{\boldsymbol{u}}}_k, \boldsymbol{u}_k - \boldsymbol{u}_{k-1} - \Delta t_{k-1}\overline{\dot{\boldsymbol{u}}}_k) \big\|_{\boldsymbol{W}_k^{\dot{u}}} \quad (12a)$$

$$l_k^{z}(\boldsymbol{z}_k) = \eta \big\| \max(\boldsymbol{0}, \boldsymbol{c}_k(\boldsymbol{z}_k)) \big\|_{\boldsymbol{W}_k^{z}} \quad (12b)$$

are added to l_k. $\|\boldsymbol{\xi}\|_{\boldsymbol{W}} = 1/2 \boldsymbol{\xi}^T \boldsymbol{W} \boldsymbol{\xi}$ defines a quadratic form and $\boldsymbol{W}_k^{\dot{u}}$ and $\boldsymbol{W}_k^{z}$ are positive semi-definite weighting matrices. Effectively, (10e) and (10f) are implemented as soft constraints only and their rigidity is tuned by $\boldsymbol{W}_k^{\dot{u}}$, $\boldsymbol{W}_k^{z}$, and the penalty parameter $\eta \gg 0$. During the solution process, η is kept constant. Implementing constraints with exterior penalty terms may cause minor violations of the original constraints. It should thus be decided on a case-by-case basis whether the entailed inaccuracy is tolerable. In this respect, it is recommendable that constraints are designed slightly more conservative, i. e., shifted inward. As an alternative, η could be continuously increased during the iterative numerical solution procedure (cf. Nocedal and Wright, 2006). In the limit case as $\eta \to \infty$, (12) has the same effect as (10e) and (10f) (cf. Wills and Heath, 2003).

Based on (11) and (12), (10) is transformed into the unconstrained problem

$$\underset{\boldsymbol{v} \in \mathbb{R}^N}{\text{minimize}} \; C(\boldsymbol{v}) = \sum_{k=\bar{K}} l_k(\boldsymbol{z}_k, \boldsymbol{\varphi}_k(\boldsymbol{v}_k)) + \frac{1}{2}\varepsilon \boldsymbol{v}_k^T \boldsymbol{v}_k + l_k^{\dot{u}}(\boldsymbol{\varphi}_k(\boldsymbol{v}_k), \boldsymbol{\varphi}_{k-1}(\boldsymbol{v}_{k-1})) + l_k^{z}(\boldsymbol{z}_k) \quad (13a)$$

$$\text{subject to } \boldsymbol{0} = \boldsymbol{f}_{k-1}(\boldsymbol{z}_k, \boldsymbol{z}_{k-1}, \boldsymbol{\varphi}_k(\boldsymbol{v}_k), \boldsymbol{\varphi}_{k-1}(\boldsymbol{v}_{k-1})), \quad k = \bar{K} \quad (13b)$$

$$\boldsymbol{z}_{k_0} = \boldsymbol{z}_0, \; \boldsymbol{\varphi}_{k_0}(\boldsymbol{v}_{k_0}) = \boldsymbol{u}_0, \quad (13c)$$

with $N = (k_1 - k_0)n$, the assembled input vector $\boldsymbol{v} = [\boldsymbol{v}_k]_{k=\bar{K}}$, and $\bar{K} = k_0 + 1, \ldots, k_1$. In contrast to the original formulation (10), there are no inequality constraints and a solution of (13) does always exist.

4.3. Numerical solution of the optimization problem

A great number of solution techniques for (13) are known (see, for instance, Bertsekas, 1999 and Polak, 1971). Among these techniques are steepest descend methods (Nocedal and Wright, 2006), conjugate gradient methods (Polak, 1971), quasi-Newton methods (Kelley and Sachs, 1987), Newton methods (Bertsekas, 1999), and trust-region methods (Nocedal and Wright, 2006). Here, the quasi-Newton method is chosen because it exhibits superlinear convergence (cf. Nocedal and Wright, 2006) and requires only the cost function $C(\boldsymbol{v})$ and its gradient $(\mathrm{d}C(\boldsymbol{v})/\mathrm{d}\boldsymbol{v})^T$ given that (13b) and (13c) hold. Fortunately, the considered system facilitates an analytical computation of this gradient, which will be discussed next.

Post-print version of the article: A. Steinboeck, D. Wild, and A. Kugi, "Nonlinear model predictive control of a continuous slab reheating furnace", *Control Engineering Practice*, vol. 21, no. 4, pp. 495–508, 2013. DOI: 10.1016/j.conengprac.2012.11.012
The content of this post-print version is identical to the published paper but without the publisher's final layout or copy editing.

Based on the Lagrange function

$$L(\boldsymbol{v}) = \boldsymbol{\mu}^T(\boldsymbol{\varphi}_{k_0}(\boldsymbol{v}_{k_0}) - \boldsymbol{u}_0) + \boldsymbol{\lambda}_{k_0}^T(\boldsymbol{z}_{k_0} - \boldsymbol{z}_0) + \sum_{k=\bar{K}} H_k(\boldsymbol{z}_k, \boldsymbol{z}_{k-1}, \boldsymbol{v}_k, \boldsymbol{v}_{k-1}, \boldsymbol{\lambda}_k)$$

with the abbreviation

$$\begin{aligned} H_k(\boldsymbol{z}_k, \boldsymbol{z}_{k-1}, \boldsymbol{v}_k, \boldsymbol{v}_{k-1}, \boldsymbol{\lambda}_k) &= l_k(\boldsymbol{z}_k, \boldsymbol{\varphi}_k(\boldsymbol{v}_k)) + \frac{1}{2}\varepsilon \boldsymbol{v}_k^T \boldsymbol{v}_k \\ &+ l_k^{\dot{u}}(\boldsymbol{\varphi}_k(\boldsymbol{v}_k), \boldsymbol{\varphi}_{k-1}(\boldsymbol{v}_{k-1})) + l_k^z(\boldsymbol{z}_k) \\ &+ \boldsymbol{\lambda}_k^T \boldsymbol{f}_{k-1}(\boldsymbol{z}_k, \boldsymbol{z}_{k-1}, \boldsymbol{\varphi}_k(\boldsymbol{v}_k), \boldsymbol{\varphi}_{k-1}(\boldsymbol{v}_{k-1})) \end{aligned}$$

and the Lagrange multipliers $\boldsymbol{\mu}$ and $\boldsymbol{\lambda}_k$ $(k = k_0, \ldots, k_1)$, the gradient can be calculated in the form

$$\left(\frac{\mathrm{d}C(\boldsymbol{v})}{\mathrm{d}\boldsymbol{v}}\right)^T = \nabla L(\boldsymbol{v}) = \left(\frac{\partial L(\boldsymbol{v})}{\partial \boldsymbol{v}}\right)^T = [\boldsymbol{g}_k]_{k=\bar{K}} \tag{14a}$$

with

$$\boldsymbol{g}_k = \left(\frac{\partial H_k}{\partial \boldsymbol{v}_k}\right)^T + \left(\frac{\partial H_{k+1}}{\partial \boldsymbol{v}_k}\right)^T, \quad k = k_0 + 1, \ldots, k_1 - 1 \tag{14b}$$

$$\boldsymbol{g}_{k_1} = \left(\frac{\partial H_{k_1}}{\partial \boldsymbol{v}_{k_1}}\right)^T \tag{14c}$$

$$\begin{aligned} \boldsymbol{0} &= \left(\frac{\partial H_k}{\partial \boldsymbol{\lambda}_k}\right)^T \\ &= \boldsymbol{f}_{k-1}(\boldsymbol{z}_k, \boldsymbol{z}_{k-1}, \boldsymbol{\varphi}_k(\boldsymbol{v}_k), \boldsymbol{\varphi}_{k-1}(\boldsymbol{v}_{k-1})), \quad k = \bar{K} \end{aligned} \tag{14d}$$

$$\boldsymbol{0} = \boldsymbol{z}_{k_0} - \boldsymbol{z}_0, \; \boldsymbol{0} = \boldsymbol{\varphi}_{k_0}(\boldsymbol{v}_{k_0}) - \boldsymbol{u}_0 \tag{14e}$$

$$\boldsymbol{0} = \left(\frac{\partial H_k}{\partial \boldsymbol{z}_k}\right)^T + \left(\frac{\partial H_{k+1}}{\partial \boldsymbol{z}_k}\right)^T, \quad k = k_0 + 1, \ldots, k_1 - 1 \tag{14f}$$

$$\boldsymbol{0} = \left(\frac{\partial H_{k_1}}{\partial \boldsymbol{z}_{k_1}}\right)^T. \tag{14g}$$

The computation of the gradient according to (14) proceeds as follows: The state trajectory $\boldsymbol{z}_k$ is solved in the conventional way in forward direction (ascending time index k) using (14d) with the initial values (14e). Then, $\boldsymbol{\lambda}_{k_1}$ is computed from (14g) and the values $\boldsymbol{\lambda}_k$ for $k \in \{k_0 + 1, \ldots, k_1 - 1\}$ are obtained in backward direction (descending time index k) from (14f). These computations are particularly simple because both (14f) and (14g) are linear equations in $\boldsymbol{\lambda}_k$. The variables $\boldsymbol{\lambda}_{k_0}$ and $\boldsymbol{\mu}$ do not need to be explicitly computed. Finally, an evaluation of (14a), (14b), and (14c) yields the gradient.

Both the memory requirements and the computational load associated with (14) can be reduced if the special structure of the continuous process is utilized (cf. (7) for the system considered in this paper). Fig. 5 indicates the behavior of the continuous process by highlighting those states that are active at some sampling point k. The corresponding overall state vector is outlined as a box on the left-hand side of the figure. In reality, many more state variables and sampling points may be required for an optimization horizon $(t_{k_0}, t_{k_1}]$. The time grid in Fig. 5 is not to scale and may be irregular.

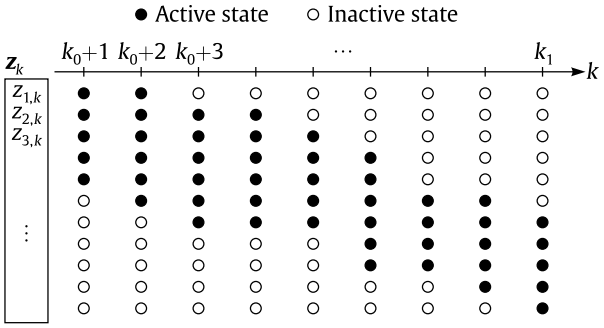

Figure 5: Active and inactive states of a continuous process.

If a state variable $z_{i,k}$ is inactive at the time t_k, it is assumed that it is in a steady state, i. e., $z_{i,k} = z_{i,k-1}$ and that it has no influence on l_k and l_k^z. It thus follows from (14f) that $\lambda_{i,k} = \lambda_{i,k-1}$ holds for the corresponding Lagrange multiplier. Moreover, (14g) shows that $\lambda_{i,k_1} = 0$ for all states i that are inactive at k_1. This shows that it suffices to compute and store $z_{i,k}$ and $\lambda_{i,k}$ only at those sampling points k where the respective state is active. Effectively, a sparse structure like that indicated by the black dots in Fig. 5 is required for the states $z_{i,k}$. For an efficient implementation, pointers should be used which demarcate the range of active states and which are appropriately increased upon incrementation of k. The same sparse memory structure is needed a second time for the Lagrange multipliers $\lambda_{i,k}$. Recall that the values $\lambda_{i,k}$ corresponding to active states are required when evaluating (14b) and (14c).

Note that H_k is not a Hamiltonian function and $\boldsymbol{\lambda}_k$ are not adjoint variables, which both would occur in a continuous-time formulation (cf. Steinboeck et al., 2011a). In the discrete-time domain, the Lagrange multipliers $\boldsymbol{\mu}$ and $\boldsymbol{\lambda}_k$ characterize the sensitivity of $C(\boldsymbol{v})$ with respect to violations of the constraints (14d) and (14e). Following this strand of thought, it is clear that $\lambda_{i,k_1} = 0$ holds for all states i that are inactive at k_1.

The necessary first-order optimality condition for the unconstrained optimization problem (13) reads as

$$\nabla L(\boldsymbol{v}) = \boldsymbol{0} \tag{15}$$

(cf. Nocedal and Wright, 2006). Any input $\boldsymbol{v}$ that satisfies (15) is a candidate for the optimum solution. Positive definiteness of the Hessian $\nabla^2 L(\boldsymbol{v})$ would serve as a sufficient second-order condition for a local optimum, but the analytical computation of $\nabla^2 L(\boldsymbol{v})$, which is in principle feasible, is a rather laborious task. It will be avoided because the quasi-Newton method yields an estimate $\boldsymbol{H}$ of the Hessian $\nabla^2 L(\boldsymbol{v})$ as a by-product anyway. It will be shown how positive definiteness of $\boldsymbol{H}$ can be enforced.

Post-print version of the article: A. Steinboeck, D. Wild, and A. Kugi, "Nonlinear model predictive control of a continuous slab reheating furnace", *Control Engineering Practice*, vol. 21, no. 4, pp. 495–508, 2013. DOI: 10.1016/j.conengprac.2012.11.012
The content of this post-print version is identical to the published paper but without the publisher's final layout or copy editing.

For the considered scenario, the quasi-Newton method works as follows:

1) Set the initial values $\boldsymbol{H}^{-1} = \boldsymbol{I}$ and $\boldsymbol{v} = \boldsymbol{0}$ and compute $\nabla L(\boldsymbol{v})$ based on (14).
2) Save $\boldsymbol{g} = \nabla L(\boldsymbol{v})$ and compute a new search direction $\boldsymbol{s} = \boldsymbol{H}^{-1}\boldsymbol{g}$.
3) Consider the abbreviations $\bar{C}(\alpha) = C(\boldsymbol{v} + \alpha\boldsymbol{s})$ and $\bar{C}'(\alpha) = \mathrm{d}C(\boldsymbol{v} + \alpha\boldsymbol{s})/\mathrm{d}\alpha$ and determine the optimum step size
$$\alpha^* = \arg\min_{\alpha\in\mathbb{R}^+} \quad \bar{C}(\alpha) \tag{16a}$$
$$\text{subject to } \bar{C}(\alpha) \leq \bar{C}(0) + r_1\bar{C}'(\alpha)\alpha \tag{16b}$$
$$\bar{C}'(\alpha) \geq r_2\bar{C}'(0) \tag{16c}$$
with constant parameters r_1 and r_2 that satisfy $0 < r_1 < r_2 < 1$.
4) Apply the update $\boldsymbol{v} \leftarrow \boldsymbol{v} + \alpha^*\boldsymbol{s}$.
5) Terminate if the current solution $\boldsymbol{v}$ is acceptable.
6) Compute the new gradient $\nabla L(\boldsymbol{v})$ based on (14) and set $\boldsymbol{d} = \nabla L(\boldsymbol{v}) - \boldsymbol{g}$.
7) Apply the BFGS update
$$\boldsymbol{H}^{-1} \leftarrow \Big(\boldsymbol{I} - \frac{\boldsymbol{s}\boldsymbol{d}^T}{\kappa}\Big)\boldsymbol{H}^{-1}\Big(\boldsymbol{I} - \frac{\boldsymbol{d}\boldsymbol{s}^T}{\kappa}\Big) + \alpha^*\frac{\boldsymbol{s}\boldsymbol{s}^T}{\kappa}$$
(cf. Nocedal and Wright, 2006) with $\kappa = \boldsymbol{d}^T\boldsymbol{s}$ and restart at step 2).

The initial value $\boldsymbol{H}^{-1} = \boldsymbol{I}$ suggested in step 1) of the above algorithm proved useful for the considered application. However, depending on the scaling of variables, assigning some other positive definite diagonal matrix to $\boldsymbol{H}^{-1}$ may give better results (cf. Nocedal and Wright, 2006). For the initial guess $\boldsymbol{v}$, practically any finite value can be chosen. If available at the respective sampling point, previously optimized values, e. g., from the previous optimization horizon, should be reused.

In step 5), various termination criteria can be implemented: The total number of iteration loops or the consumed computing time can be limited, $C(\boldsymbol{v})$ may be required to decrease by less than a certain (relative) value, or $C(\boldsymbol{v})$ or some norm of $\alpha^*\boldsymbol{s}$ may be required to fall below a threshold. For the problem considered in this paper, executing the algorithm for a fixed number of iteration loops proved simple and most useful. Then, the available computation time, i. e., the sampling period of the model predictive controller, is well utilized.

Step 3) of the algorithm, which yields the optimum step size α^*, is known as line search (Bertsekas, 1999; Nocedal and Wright, 2006). Typically, this subordinate, 1-dimensional optimization problem is only approximately solved, e. g., by a point-by-point search or by fitting a quadratic polynomial. The inequality constraints (16b) and (16c) are known as Wolfe conditions. They ensure that the so-called curvature condition
$$\boldsymbol{d}^T\boldsymbol{s} > 0 \tag{17}$$
(cf. Nocedal and Wright, 2006) is satisfied in each iteration loop, which implies positive definiteness of $\boldsymbol{H}^{-1}$. Note that κ/α^* is (approximately) the curvature of $\bar{C}(\alpha)$. Since $\boldsymbol{H}$ is a local approximation of $\nabla^2 L(\boldsymbol{v})$, it is plausible—though not guaranteed—that enforcing (17) will steer the algorithm to a minimum where the sufficient second-order optimality condition (positive definiteness of $\nabla^2 L(\boldsymbol{v})$) is satisfied. Conditions for the optimization problem that would guarantee the BFGS method to converge to such a minimum are given, for instance, in (Fletcher, 1984; Nocedal and Wright, 2006).

The quasi-Newton method was chosen for solving the dynamic optimization problem (13) because it is easily implemented, ensures frugal memory usage, and achieves superlinear convergence. In the following section, the optimization problem is further tailored to the furnace control scenario.

4.4. Parameterization for the furnace control problem

The objectives and constraints of the furnace control problem from Section 3.2 are reformulated such that they are compatible with the optimization problem (10). The main control objective is to reheat the slabs to their desired final temperature profiles. It is implemented by means of the cost function
$$l_k(\boldsymbol{x}_k, \boldsymbol{u}_k) = \sum_j \delta_{k,k_{j,1}} \big\|\boldsymbol{x}_{j,k} - \tilde{\boldsymbol{x}}_{j,end}\big\|_{\boldsymbol{W}^{x_{end}}} w_j. \tag{18}$$
$\boldsymbol{W}^{x_{end}}$ is a (usually diagonal) positive definite weighting matrix that penalizes the final control error of the slab temperature profiles. The weighting factor w_j was defined in Table 1 and may, for instance, depend on the economic value of the slab. The cost function l_k could also depend on the input $\boldsymbol{u}_k$ but in the current analysis this option is not used.

Since the slab temperature profile $T_j(y,t)$ is a function of the state $\boldsymbol{x}_{j,k}$, the constraints (8) (see also Fig. 3) can be realized by means of (10f), which is finally implemented in the penalty term (12b). Again, the weighting factor w_j may enter this expression. The remaining input constraints (9) are directly compatible with (10d) and (10e), which are considered by the nonlinear map (11) and by the penalty term (12a), respectively.

At any sampling point k, the cost function (cf. (13a)) depends, apart from the inputs $\boldsymbol{v}_k$ and $\boldsymbol{v}_{k-1}$, only on the states of those slabs that are currently inside the furnace. The state-space system (7) has already the same format as (10b); effectively, only the subsystem (6) relevant for active states has to be implemented. Hence, the problem formulation results indeed in a structure of a continuous process and the sparse implementation indicated in Fig. 5 can be employed.

The weighting matrices $\boldsymbol{W}_k^{\dot{u}}$, $\boldsymbol{W}_k^{z}$, and $\boldsymbol{W}^{x_{end}}$ are empirically found. Finally, the time grid for executing the controller has to be defined. For the furnace control problem, the overlapping optimization horizons should be at least 3 h long. This lower bound value for the horizon length corresponds to the system dynamics insofar as the

Post-print version of the article: A. Steinboeck, D. Wild, and A. Kugi, "Nonlinear model predictive control of a continuous slab reheating furnace", *Control Engineering Practice*, vol. 21, no. 4, pp. 495–508, 2013. DOI: 10.1016/j.conengprac.2012.11.012
The content of this post-print version is identical to the published paper but without the publisher's final layout or copy editing.

influence of an input $\boldsymbol{u}_k$ applied at the time t_k decreases to a practically negligible level before $t_k + 3\,\mathrm{h}$. The sampling period of the model predictive controller should not be longer than 5 min. The same applies to sampling periods used for integrating the system, i. e., $\Delta t_k \leq 5\,\mathrm{min}$. Clearly, these are crucial design parameters which have an impact on both control accuracy and computational load.

4.5. On-line adaptation of constraints

Strictly speaking, the inputs $\boldsymbol{u}_k$, i. e., the zone temperatures, are system states themselves, which is, for instance, reflected in the more sophisticated furnace models of Ko et al. (2000); Wild et al. (2009); and Yoshitani et al. (1994). However, this fact is neglected in the considered furnace and $\boldsymbol{u}_k$ is used as input. This simplification helps to minimize the complexity of the control concept. In fact, the assumption $\tilde{\boldsymbol{u}}_k = \boldsymbol{u}_k$ is supposed to hold as long as the constraints (9) are satisfied. The validity of this assumption is now explored in more depth and harmonized with theoretical considerations.

It is plausible that the constraint values $\underline{\boldsymbol{u}}_k$, $\overline{\boldsymbol{u}}_k$, $\underline{\dot{\boldsymbol{u}}}_k$, and $\overline{\dot{\boldsymbol{u}}}_k$ depend on the heating capacity of the furnace and the current operational situation, especially the current stock of slabs inside the furnace. Measurement results from the real system confirmed this expectation. They showed that nominal constraint values accurately define the performance frontiers of the system only if all subordinate control loops (PI zone controllers in Fig. 2) work properly, i. e., if their respective constraints are inactive. On the contrary, if subordinate control loops are saturated, e. g., if constraints on the fuel flow rates to the burners are active, the nominal bounds $\underline{\boldsymbol{u}}_k$, $\overline{\boldsymbol{u}}_k$, $\underline{\dot{\boldsymbol{u}}}_k$, and $\overline{\dot{\boldsymbol{u}}}_k$ are effectively too lax.

These observations sparked the idea of making the constraints $\underline{\boldsymbol{u}}_k$, $\overline{\boldsymbol{u}}_k$, $\underline{\dot{\boldsymbol{u}}}_k$, and $\overline{\dot{\boldsymbol{u}}}_k$ adaptive depending on the current state of subordinate control loops. The constraints are adapted right at the beginning of each call of the model predictive control algorithm, i. e., at each sampling point and before solving the dynamic optimization problem. This heuristic adaptation method is individually applied to each furnace zone. In an exemplary fashion, the algorithm is outlined for zone i in the top half of the furnace at the sampling point k_0, i. e., at the beginning of an optimization horizon:

1) Measure the current real furnace zone temperature $T^+_{z,i}(t_{k_0})$ by means of thermocouples installed inside the furnace and compute the control error $T^+_{z,i}(t_{k_0}) - \tilde{T}^+_{z,i}(t_{k_0})$ of the subordinate PI control loop.
2) If $|T^+_{z,i}(t_{k_0}) - \tilde{T}^+_{z,i}(t_{k_0})| < \Delta T^+_{z,i,sat}$, set $\underline{T}^+_{z,i,k}$, $\overline{T}^+_{z,i,k}$, $\underline{\dot{T}}^+_{z,i,k}$, and $\overline{\dot{T}}^+_{z,i,k}$ to their nominal values and continue with step 4).
3) Otherwise, set the constraints $\underline{T}^+_{z,i,k}$, $\overline{T}^+_{z,i,k}$, $\underline{\dot{T}}^+_{z,i,k}$, and $\overline{\dot{T}}^+_{z,i,k}$ to more restrictive values depending on the sign and magnitude of $T^+_{z,i}(t_{k_0}) - \tilde{T}^+_{z,i}(t_{k_0})$. Consider, for instance, that the fuel supply suffers upper-bound saturation, which causes $\tilde{T}^+_{z,i}(t_{k_0}) - T^+_{z,i}(t_{k_0}) > \Delta T^+_{z,i,sat}$. Then, $\overline{T}^+_{z,i,k}$ and $\overline{\dot{T}}^+_{z,i,k}$ should be reduced whereas $\underline{T}^+_{z,i,k}$ and $\underline{\dot{T}}^+_{z,i,k}$ should be assigned their nominal values.
4) Based on $T^+_{z,i}(t_{k_0})$ and the updated parameters $\underline{T}^+_{z,i,k}$, $\overline{T}^+_{z,i,k}$, $\underline{\dot{T}}^+_{z,i,k}$, and $\overline{\dot{T}}^+_{z,i,k}$, compute new effective bounds $\underline{T}^+_{z,i,k}$ and $\overline{T}^+_{z,i,k}$ as indicated in Fig. 6.

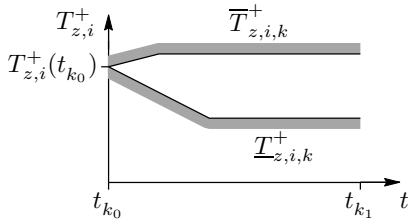

Figure 6: On-line adaptation of input constraints.

In step 2) of the algorithm, the observed control error $T^+_{z,i}(t_{k_0}) - \tilde{T}^+_{z,i}(t_{k_0})$ and a system-specific threshold $\Delta T^+_{z,i,sat}$ are used to assess the current condition of the subordinate control loop. As an alternative, this information could be directly obtained from the respective PI controller. Step 4) describes the computation of effective constraints shown in Fig. 6. The sloping sections of these constrains are defined according to $\underline{\dot{T}}^+_{z,i,k}$ and $\overline{\dot{T}}^+_{z,i,k}$.

The proposed method has another significant advantage: It ensures the initial slope of the optimized input to be exactly within the allowed range $[\underline{\dot{\boldsymbol{u}}}_k, \overline{\dot{\boldsymbol{u}}}_k]$. Thus, the adaptation algorithm can restore exact compliance with the constraints (9b), despite their implementation as soft constraints.

5. Example problem

In the following simulation study, the mathematical model of Wild et al. (2009) is used to simulate the real furnace. Measurement results validating this model and comparing it to the model developed in Section 2 are presented in (Steinboeck et al., 2010).

The simulations are required for several reasons: First, not all interesting features and capabilities of the control algorithm can actually be tested in a real plant (cf. Section 6), e. g., due to operational constraints. Second, the simulations had been extensively used for testing, tuning, and verifying the model predictive controller before it was commissioned. Therefore, the simulation environment contains an implementation of the developed model predictive controller and emulators of the process controller and the PI zone controllers shown in Fig. 2.

In the current section, two simulated steady-state scenarios with the desired final temperature profiles shown in Fig. 7 are analyzed. In a steady-state scenario, all slabs have the same material, the same size (thickness $D_j = 0.35\,\mathrm{m}$), the same initial temperature (homogenous profile $T_{j,0}(y) = 330\,\mathrm{K}$), the same desired final temperature, and the same reheating time ($t_{j,1} - t_{j,0} = 6\,\mathrm{h}$). The

Post-print version of the article: A. Steinboeck, D. Wild, and A. Kugi, "Nonlinear model predictive control of a continuous slab reheating furnace", *Control Engineering Practice*, vol. 21, no. 4, pp. 495–508, 2013. DOI: 10.1016/j.conengprac.2012.11.012

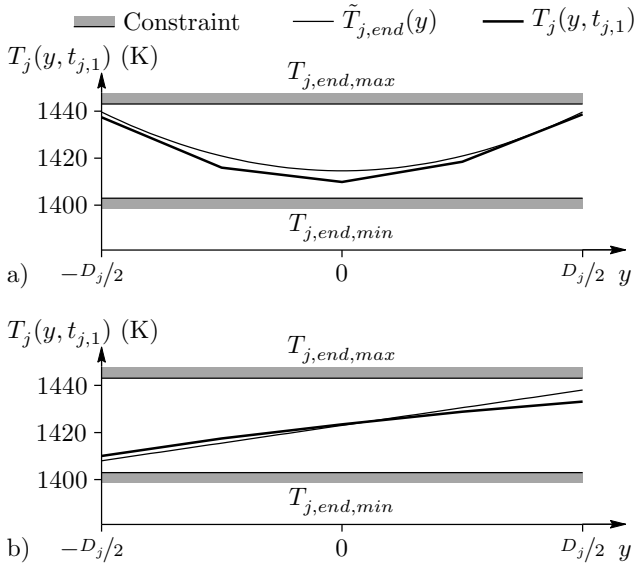

Figure 7: Final slab temperature profile (from simulation), a) symmetric, b) asymmetric.

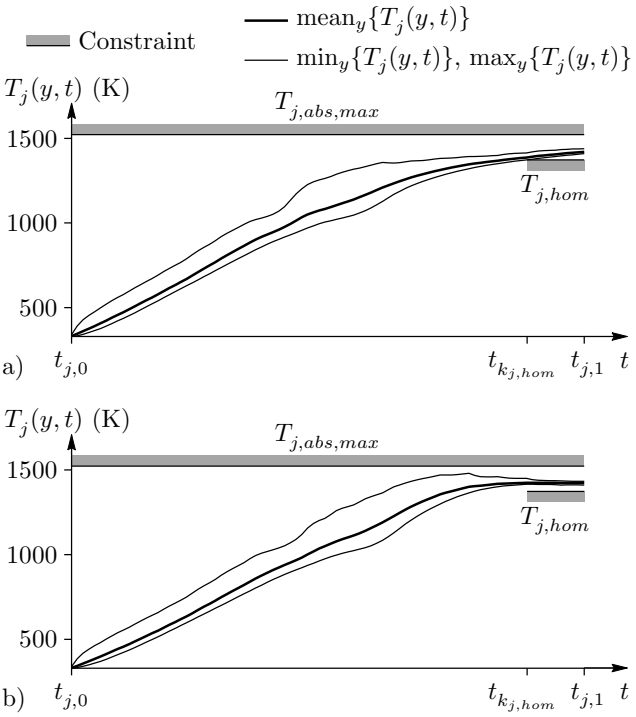

Figure 8: Slab temperature trajectories (from simulation), a) symmetric final slab temperature profile, b) asymmetric final slab temperature profile.

furnace contains 18 slabs at a time and the slabs are discharged at 0.33 h intervals. The system states are not constant but the furnace operation is periodic with the period 0.33 h, i. e., the period is equivalent to the time between two slab discharging events.

The desired temperature profiles in Fig. 7 are purely user-defined. On the contrary, the corresponding reheating trajectories, which are shown in Fig. 8, are a result of the optimization-based controller.

In the first scenario (Figs. 7a and 8a), the slabs are reheated to a symmetric temperature profile $\tilde{T}_{j,end}(y)$ defined by $\tilde{\boldsymbol{x}}_{j,end} = [1423\,\text{K}, 0\,\text{K}, 25\,\text{K}]^T$. That is a non-stationary temperature profile, where the surface temperature should be 25 K higher than the core temperature and $^2/_3\,25$ K higher than the slab mean temperature. Hence, the mean temperature is rising, which is corroborated by Fig. 8a.

In the second scenario (Figs. 7b and 8b), the slabs should be reheated to an asymmetric, inhomogeneous temperature profile $\tilde{T}_{j,end}(y)$ defined by $\tilde{\boldsymbol{x}}_{j,end} = [1423\,\text{K}, 15\,\text{K}, 0\,\text{K}]^T$. This means that the top slab surface temperature should be 30 K higher than the bottom slab surface temperature. All other parameters are the same as before. The final temperature profile of the second scenario is stationary, which implies that the final slab mean temperature is constant. This is confirmed by the horizontal tangent at the end of the trajectory shown in Fig. 8b.

As can be inferred from Figs. 7 and 8, the slabs are accurately reheated and no constraints are violated. In none of the two scenarios, the subordinate PI zone controllers are saturated. Saturation of subordinate control loops could limit the control performance. Such problems would, for instance, occur if the desired final slab temperature profile were concave (surface temperature below core temperature), instead of convex like in the first scenario. The reason for this limitation is that the furnace does not have any cooling facilities. The current simulation study shows that the proposed model predictive controller can reheat slabs accurately and without violation of constraints.

6. Measurement results

The control system shown in Fig. 2 belongs to an industrial slab reheating furnace of Aktiengesellschaft der Dillinger Hüttenwerke. There, the model predictive controller from Section 4 has been implemented as a C++ program. It was commissioned in February 2011 and has been in permanent operation since then.

The current section summarizes measurement results from the real furnace system. There, a Kalman filter developed by Wild (2010); Wild et al. (2007) is used as a state observer (cf. Fig. 2) for non-measurable quantities. The high accuracy of this observer was validated by means of a test slab that was instrumented with thermocouples and reheated in the considered furnace. Among the estimated quantities are the slab temperatures presented in the following.

The considered furnace operates usually under non-steady-state conditions because the slabs vary in terms of geometry, material, reheating time, initial temperature $T_{j,0}(y)$, and desired final temperature $\tilde{T}_{j,end}$. The

Post-print version of the article: A. Steinboeck, D. Wild, and A. Kugi, "Nonlinear model predictive control of a continuous slab reheating furnace", *Control Engineering Practice*, vol. 21, no. 4, pp. 495–508, 2013. DOI: 10.1016/j.conengprac.2012.11.012
The content of this post-print version is identical to the published paper but without the publisher's final layout or copy editing.

slabs should finally reach a temperature profile defined by $\tilde{\boldsymbol{x}}_{j,end} = [\tilde{T}_{j,end}, 0, 0]^T$, i. e., a homogeneous temperature profile. For the model predictive controller, relatively conservative constraint values $T_{j,hom} = T_{j,end,min} = \tilde{T}_{j,end} - 15\,\mathrm{K}$ and $T_{j,end,max} = \tilde{T}_{j,end} + 15\,\mathrm{K}$ are used. In reality, the subsequent rolling process does not require such restrictive constraints. The reasons for the conservative choices are that the real slab temperatures are not exactly uniform along the width and the length of the slabs (directions orthogonal to y) and that the Kalman filter may entail inaccuracies of the estimated slab temperatures. Potential causes of these generally small inaccuracies (cf. Wild, 2010; Wild et al., 2007) are model mismatches and uncertain material parameters.

The considered furnace is 35.1 m long, 12.5 m wide, and up to 7.5 m high. It can reheat slabs with thicknesses ranging from 0.15 m to 0.45 m. Depending on the product dimensions, the furnace is typically charged with 30 to 60 slabs at a time. Though, the furnace normally reheats two parallel rows of slabs, they are conceptually aggregated for control purposes to a single row of representative slabs. This seems justified because of the absence of control facilities for each individual row. An alternative concept that can individually control parallel rows was reported by Shenvar (1994).

The analysis starts with a brief look on the furnace zone temperatures. For a representative period, Fig. 9 shows these temperatures for zone 3. Since the graph contains both the reference signals and the measured values, it reveals the control accuracy achieved by the subordinate PI zone controllers. As can be seen from Fig. 9, the constraints on $T^{\mp}_{z,3}(t)$ and $\dot{T}^{\mp}_{z,3}(t)$ are sufficiently respected. The signals for the other furnace zones exhibit a similar

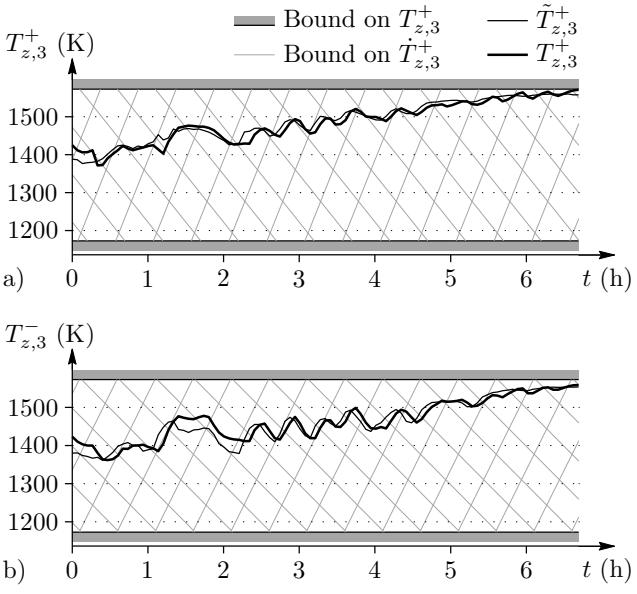

Figure 9: Furnace temperatures in zone 3, a) top half of furnace, b) bottom half of furnace.

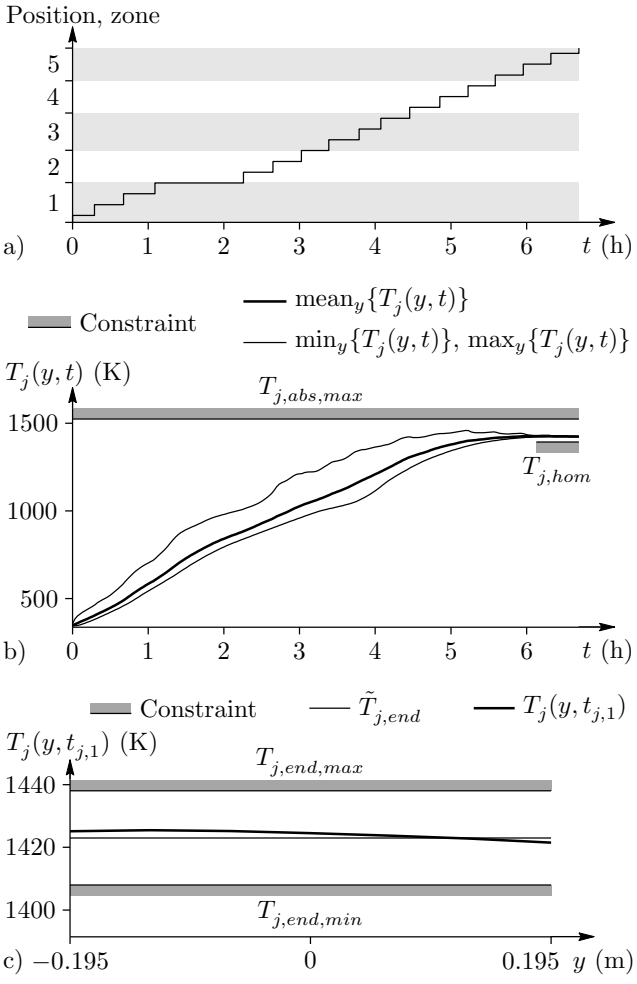

Figure 10: Trajectories of a typical slab (index $j = 77$), a) path-time diagram, b) reheating trajectory, c) final temperature profile.

behavior.

Next, the results of a single slab with the index $j = 77$ are studied. This typical slab was reheated exactly during the period covered by Fig. 9. Fig. 10 shows the path-time diagram, the reheating trajectory, and the final temperature profile of the slab. It is $D_j = 0.39\,\mathrm{m}$ thick and was reheated for 6.7 h. Fig. 10a indicates that the path-time diagrams of slabs can be fairly irregular. Stopping the reheating process for a time of 1 h or more, is not an uncommon event. These interruptions are usually caused by up- or downstream process steps and have some influence on the slab reheating trajectories (cf. Fig. 10b). Fig. 10 shows that the considered slab satisfies all relevant constraints ($T_{j,abs,max}$, $T_{j,hom}$, $T_{j,end,min}$, and $T_{j,end,max}$), accurately reaches its desired final temperature $\tilde{T}_{j,end}$, and has a sufficiently homogeneous final temperature profile.

In a further step, it is analyzed whether the high control accuracy observed in Fig. 10 is consistently achieved. Therefore, the final slab temperatures, their desired values, and their allowed ranges are shown in Fig. 11 for slabs

Post-print version of the article: A. Steinboeck, D. Wild, and A. Kugi, "Nonlinear model predictive control of a continuous slab reheating furnace", *Control Engineering Practice*, vol. 21, no. 4, pp. 495–508, 2013. DOI: 10.1016/j.conengprac.2012.11.012

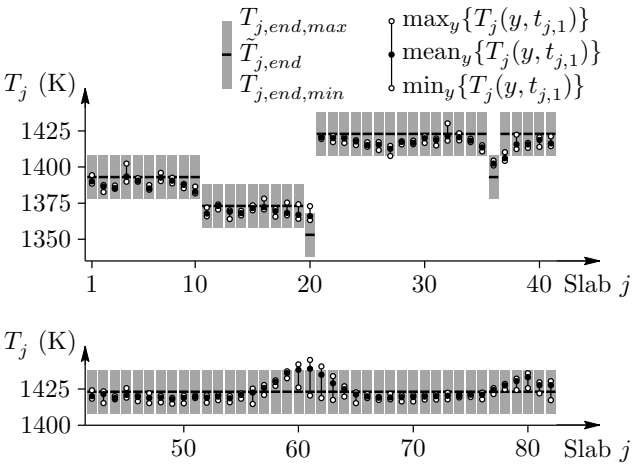

Figure 11: Final temperature ranges of slabs.

that are successively discharged from the furnace. It can be inferred from this figure that the control performance in terms of the final slab temperatures is satisfactory. The majority of slabs are reheated without any violations of the constraints $T_{j,abs,min}$ and $T_{j,abs,max}$. If such violations occur like for the slabs $j = 20$, $j = 37$, as well as $j = 60$ and its neighbors (cf. Fig. 11), there may be three main causes: The allocated reheating time may be inappropriate for the respective thickness of the slabs, the allowed temperature ranges of neighboring slabs do not sufficiently overlap, or the supervisory process controller modified the production schedule at too short notice, e. g., due to unforeseen events in other process steps.

The results are further consolidated by studying the frequency distributions of control errors. A sample of 7025 slabs reheated by the new model predictive controller is compared with a sample of 5278 slabs processed during the last months of the previous controller. The latter materialized a zone-based PI control concept similar to those proposed by Ditzhuijzen et al. (2002); Fontana et al. (1983); and Shenvar (1994).

Fig. 12 shows the frequency density of the mean final slab temperature error $\mathrm{mean}_y\{T_j(y,t_{j,1})\} - \tilde{T}_{j,end}$. Some

Table 2: Comparison of control performance in terms of the final control error $T_j(y,t_{j,1}) - \tilde{T}_{j,end}$.

Aggregate error quantity	Previous controller	New model predictive controller
Mean	13.0 K	0.9 K
Standard deviation	12.3 K	9.4 K
Median	13.2 K	−0.6 K

statistical key figures of this error are given in Tab. 2. Clearly, the previous controller reheated the slabs too much.

The distribution of the control error of the previous controller (white bars in Fig. 12) is similar to a normal distribution, which hints at a random control error. On the contrary, the corresponding distribution for the new model predictive controller (black bars in Fig. 12) is relatively narrow and asymmetric, which can be attributed to the superior accuracy and the systematic objectives of this controller. The distribution is asymmetric because violations of the lower bounds $T_{j,hom}$ and $T_{j,end,min}$ are more heavily punished than violations of the upper bound $T_{j,end,max}$ ($T_{j,abs,max}$ is practically never violated). This strategy is tailored to the requirements of the subsequent rolling process. The asymmetry of the distribution obtained with the new controller is underlined by the large difference between mean and median values given in Tab. 2.

The previous controller reheated slabs to a temperature that exceeded the target value on average by 13.0 K. With the new controller, this mean error has been reduced to 0.9 K. The standard deviation of the error has also been reduced (cf. Tab. 2). This indicates that the new controller achieves a higher accuracy and that it facilitates smaller safety margins for the final slab temperature. In fact, overheating of slabs in exchange for less frequent violations of the lower bounds $T_{j,hom}$ and $T_{j,abs,max}$, which was often used with the previous controller, is no longer required with the new one. The new controller improves the product quality in two respects: reduced scale formation and less frequent overheating.

Fig. 13 shows the frequency distribution of violations

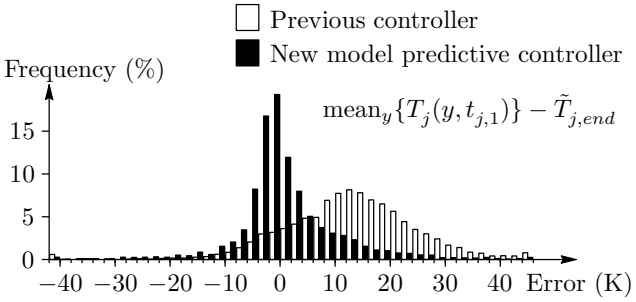

Figure 12: Frequency density of control errors in terms of final slab mean temperatures.

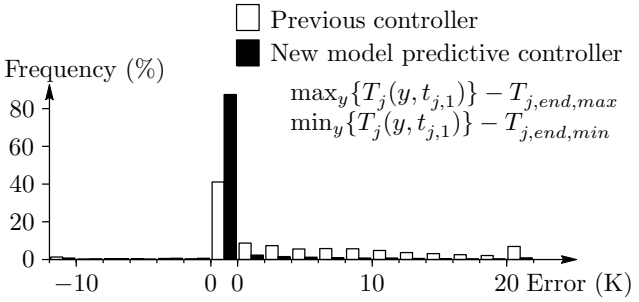

Figure 13: Frequency density of control errors in terms of bounds on final slab temperature profiles.

Post-print version of the article: A. Steinboeck, D. Wild, and A. Kugi, "Nonlinear model predictive control of a continuous slab reheating furnace", *Control Engineering Practice*, vol. 21, no. 4, pp. 495–508, 2013. DOI: 10.1016/j.conengprac.2012.11.012
The content of this post-print version is identical to the published paper but without the publisher's final layout or copy editing.

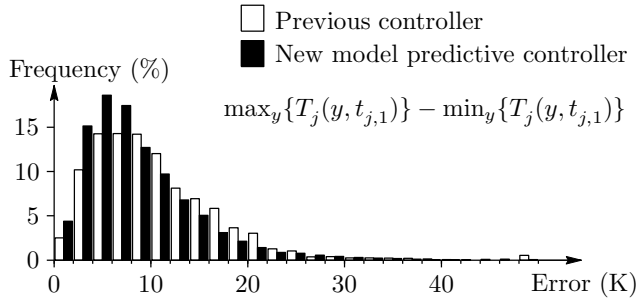

Figure 14: Frequency density of inhomogeneities of final slab temperature profiles.

of the bounds $T_{j,end,min}$ and $T_{j,end,max}$. This figure confirms the good results of the new controller. On average, 88 % of the slabs leave the furnace with a temperature profile that is completely within the desired range $[T_{j,end,min}, T_{j,end,max}]$. That is, the error rate is as low as 12 %. The previous controller had an error rate of 59 %. However, these numbers are not representative for the real reject rates because $T_{j,end,min}$ and $T_{j,end,max}$ were chosen overly conservative. In Figs. 12, 13, and 14, the left-most and right-most histogram bins may have different widths than the other bins.

The frequency distribution of the inhomogeneities $\max_y\{T_j(y,t_{j,1})\} - \min_y\{T_j(y,t_{j,1})\}$ of the final slab temperature profiles is shown in Fig. 14. Clearly, a distribution that tends more towards the left is preferable because the final slab temperature profiles should be uniform. The new model predictive controller incorporates this objective by the cost term (18), which minimizes the second and the third component of $\boldsymbol{x}_{j,k_{j,1}}$ (recall that $\tilde{\boldsymbol{x}}_{j,end} = [\tilde{T}_{j,end}, 0, 0]^T$). In fact, the new controller actively homogenizes the final slab temperature profiles, which is supported by Fig. 14. These results confirm once more that the new model predictive controller performs better than its predecessor.

7. Conclusions

A nonlinear model predictive controller for a continuous slab reheating furnace was designed. A tailored mathematical model and an efficient time-integration method turned out to be mandatory to ensure that the dynamic optimization problem can be (iteratively) solved in real time. These requirements can be achieved by means of the Galerkin weighted residual method for the heat conduction problem, a tractable formulation of radiative and convective heat transfer, and an implicit time integration assuming piecewise linear heat flows into the slabs. With the Galerkin method, both active homogenization and reaching desired final slab temperature profiles is feasible.

A finite-time constrained optimization problem was formulated based on control objectives, operational constraints, and knowledge of future events. Incorporating such future knowledge is particularly important for systems with large time constants like a slab reheating furnace. Generally, the existence of a solution of the original constrained optimization problem cannot be guaranteed, which is why it was reformulated as an unconstrained optimization problem. It is efficiently solved by means of the quasi-Newton method with the BFGS update formula.

The special structure of the continuous process was systematically exploited to keep the computational load and memory requirements of the optimization problem at moderate levels. This methodology is transferable to many other continuous production processes.

The achieved control accuracy benefits significantly from an on-line adaptation of input constraints depending on the current state of the subordinate control loops. This approach facilitates that subordinate control loops are operated at their effective performance frontiers. It does not require an extension of the model or additional computational resources. Moreover, the approach allows the model predictive controller to cope with non-ideal subordinate control loops in a cascade structure.

Results from a full-scale industrial application of the controller have demonstrated that the achieved control accuracy is significantly higher than with the previous zone-based PI control concept. The good control performance has been evidenced both at the level of individual slabs and at an aggregate level with a sample size of more than 7000 slabs. Encouraged by these results, the control system has also been installed on two other continuous slab reheating furnaces in the same plant.

8. Acknowledgements

The authors from Vienna University of Technology gratefully acknowledge ongoing useful advice and financial support by Aktiengesellschaft der Dillinger Hüttenwerke.

References

Balbis, L., Balderud, J., and Grimble, M. (2008). Nonlinear predictive control of steel slab reheating furnace. In *Proceedings of the American Control Conference, Seattle, Washington, USA*, 1679–1684.

Bertsekas, D. (1999). *Nonlinear Programming*. Athena Scientific, Belmont, Massachusetts, 2nd edition.

BISRA (1953). Physical constants of some commercial steels at elevated temperatures. Technical report, British Iron & Steel Research Association, London.

Camacho, E. and Bordons, C. (2004). *Model Predictive Control*. Advanced Textbooks in Control and Signal Processing. Springer, London, Berlin, 2nd edition.

Chen, S. (2009). *Flat-Rolled Steel Processes: Advanced Technologies*, chapter Modeling for Reheat Furnace Practices, 99–114. CRC Press, Boca Raton.

Choi, J., Jang, Y., and Kim, S. (2001). Temperature control of a reheating furnace using feedback linearization and predictive control. In *Proceedings of the International Conference on Control, Automation and Systems, ICCAS 2001, Jeju, Korea*, 103–106.

Ditzhuijzen, G., Staalman, D., and Koorn, A. (2002). Identification and model predictive control of a slab reheating furnace. In *Proceedings of the 2002 IEEE International Conference on Control Applications, Glasgow, UK*, 361–366.

Post-print version of the article: A. Steinboeck, D. Wild, and A. Kugi, "Nonlinear model predictive control of a continuous slab reheating furnace", *Control Engineering Practice*, vol. 21, no. 4, pp. 495–508, 2013. DOI: 10.1016/j.conengprac.2012.11.012
The content of this post-print version is identical to the published paper but without the publisher's final layout or copy editing.

Findeisen, R., Allgöwer, F., and Biegler, L. (eds.) (2007). *Assessment and Future Directions of Nonlinear Model Predictive Control*, volume 358 of *Lecture Notes in Control and Information Sciences*. Springer, Berlin.

Fletcher, C. (1984). *Computational Galerkin Methods*. Springer, New York.

Fontana, P., Boggiano, A., Furinghetti, A., Cabras, G., and Simoncini, C. (1983). An advanced computer control system for reheat furnaces. *Iron and Steel Engineer*, 60(8), 55–62.

Fujii, S., Urayama, K., Kashima, K., Imura, J., Kurokawa, T., and Adachi, S. (2010). Machine-based modeling of conveyor-type flowshops with application to scheduling and temperature control in slab reheating furnace. In *Proceedings of the 2010 IEEE International Conference on Control Applications, Yokohama, Japan*, 2059–2064.

Giselsson, P. (2010). Adaptive nonlinear model predictive control with suboptimality and stability guarantees. In *Proceedings of the IEEE Conference on Decision and Control, Atlanta, GA, USA*, 3644–3649.

Graichen, K. and Kugi, A. (2010). Stability of incremental model predictive control without terminal constraints. *IEEE Transactions on Automatic Control*, 55(11), 2576–2580.

Graichen, K. and Petit, N. (2008). Constructive methods for initialization and handling mixed state-input constraints in optimal control. *Journal of Guidance, Control, and Dynamics*, 31(5), 1334–1343.

Graichen, K. and Petit, N. (2009). Incorporating a class of constraints into the dynamics of optimal control problems. *Optimal Control Applications and Methods*, 30(6), 537–561.

Grüne, L. (2009). Analysis and design of unconstrained nonlinear MPC schemes for finite and infinite dimensional systems. *SIAM Journal on Control and Optimization*, 48(2), 1205–1228.

Grüne, L. and Pannek, J. (2011). *Nonlinear Model Predictive Control*. Springer, London.

Han, S., Chang, D., and Kim, C. (2010). A numerical analysis of slab heating characteristics in a walking beam type reheating furnace. *International Journal of Heat and Mass Transfer*, 53, 3855–3861.

Icev, Z., Zhao, J., Stankovski, M., Kolemisevska-Gugulovska, T., and Dimirovski, G. (2004). Supervisory-plus-regulatory control design for efficient operation of industrial furnaces. *Journal of Electrical & Electronics Engineering*, 4(2), 1199–1218.

Kays, W., Crawford, M., and Weigand, B. (2005). *Convective Heat and Mass Transfer*. McGraw Hill, New York, 4$^{\text{th}}$ edition.

Keerthi, S. and Gilbert, E. (1985). An existence theorem for discrete-time infinite-horizon optimal control problems. *IEEE Transactions on Automatic Control*, 30(9), 907–909.

Kelley, C. and Sachs, E. (1987). Quasi-newton methods and unconstrained optimal control problems. *SIAM Journal on Control and Optimization*, 25, 1503–1516.

Kim, J., Huh, K., and Kim, I. (2000). Three-dimensional analysis of the walking-beam-type slab reheating furnace in hot strip mills. *Numerical Heat Transfer, Part A*, 38, 589–609.

Ko, H., Kim, J., Yoon, T., Lim, M., Yang, D., and Jun, I. (2000). Modeling and predictive control of a reheating furnace. In *Proceedings of the American Control Conference, Chicago, Illinois, USA*, volume 4, 2725–2729.

Marino, P., Pignotti, A., and Solis, D. (2004). Control of pusher furnaces for steel slab reheating using a numerical model. *Latin Amercian Applied Research*, 34(4), 249–255.

Modest, M. (2003). *Radiative Heat Transfer*. Academic Press, New York, 2$^{\text{nd}}$ edition.

Nederkoorn, E., Wilgen, P., and Schuurmans, J. (2011). Nonlinear model predictive control of walking beam furnaces. In *Proceedings of the 1st International Conference on Energy Efficiency and CO_2 Reduction in the Steel Industry, EECR STEEL, Düsseldorf, Germany*.

Nocedal, J. and Wright, S. (2006). *Numerical Optimization*. Springer Series in Operations Research. Springer, New York, 2$^{\text{nd}}$ edition.

Pannek, J. and Worthmann, K. (2011). Reducing the prediction horizon in NMPC: An algorithm based approach. In *Proceedings of the 18th World Congress of the International Federation of Automatic Control (IFAC), Milan, Italy*, 7969–7974.

Pike, H. and Citron, S. (1970). Optimization studies of a slab reheating furnace. *Automatica*, 6, 41–50.

Polak, E. (1971). *Computational Methods in Optimization: A Unified Approach*, volume 77 of *Mathematics in Science and Engineering*. Academic Press, New York.

Reble, M. and Allgöwer, F. (2012). Unconstrained model predictive control and suboptimality estimates for nonlinear continuous-time systems. *Automatica*, 48(8), 1812–1817.

Shenvar, F. (1994). Walking beam furnace supervisory control at Inland's 80-in. hot strip mill. *Iron and Steel Engineer*, 71(7), 25–34.

Siegel, R. and Howell, J. (2002). *Thermal Radiation Heat Transfer*. Taylor & Francis, New York, London, 4$^{\text{th}}$ edition.

Stadler, K., Poland, J., and Gallestey, E. (2011). Model predictive control of a rotary cement kiln. *Control Engineering Practice*, 19(1), 1–9.

Steinboeck, A., Graichen, K., and Kugi, A. (2011a). Dynamic optimization of a slab reheating furnace with consistent approximation of control variables. *IEEE Transactions on Control Systems Technology*, 16(6), 1444–1456.

Steinboeck, A., Graichen, K., Kugi, A., and Wild, D. (2011b). A mathematical model of a slab reheating furnace for simulation, control, and optimization. In *Proceedings of the 4th International Conference on Modelling and Simulation of Metallurgical Processes in Steelmaking, STEELSIM, Düsseldorf, Germany*.

Steinboeck, A., Graichen, K., Wild, D., Kiefer, T., and Kugi, A. (2011c). Model-based trajectory planning, optimization, and open-loop control of a continuous slab reheating furnace. *Journal of Process Control*, 21(2), 279–292.

Steinboeck, A., Wild, D., Kiefer, T., and Kugi, A. (2010). A mathematical model of a slab reheating furnace with radiative heat transfer and non-participating gaseous media. *International Journal of Heat and Mass Transfer*, 53, 5933–5946.

Steinboeck, A., Wild, D., and Kugi, A. (2011d). Feedback tracking control of continuous reheating furnaces. In *Proceedings of the 18th World Congress of the International Federation of Automatic Control (IFAC), Milan, Italy*, 11744–11749.

Sugiyama, S.I., Ishii, T., Ishioka, M., Hino, Y., and Okawa, T. (1999). Schedule-free heating in preheating furnace. *NKK Technical Review*, 80, 35–45.

Wang, W., Li, H.X., and Zhang, J. (2003). A hybrid approach for supervisory control of furnace temperature. *Control Engineering Practice*, 11(11), 1325–1334.

Wang, Z., Wu, Q., and Chai, T. (2004). Optimal-setting control for complicated industrial processes and its application study. *Control Engineering Practice*, 12, 65–74.

Wild, D. (2010). *Modellierung und Beobachterentwurf für einen Stoßofen*. Ph.D. thesis, Vienna University of Technology, Austria, Shaker: Aachen, Germany.

Wild, D., Meurer, T., and Kugi, A. (2009). Modelling and experimental model validation for a pusher-type reheating furnace. *Mathematical and Computer Modelling of Dynamical Systems*, 15(3), 209–232.

Wild, D., Meurer, T., Kugi, A., Fichet, O., and Eberwein, K. (2007). Nonlinear observer design for pusher-type reheating furnaces. In *Proceedings of the 3rd International Steel Conference on New Developments in Metallurgical Process Technologies, Düsseldorf, Germany*, 790–797.

Wills, A. and Heath, W. (2003). An exterior/interior-point approach to infeasibility in model predictive control. *Proceedings of the 42th IEEE Conference on Decision and Control, Maui, Hawaii, USA*, 3701–3705.

Wörk, A. (1971). Optimal control of slab reheating furnaces. In *Proceedings of the IFAC Symposium on the control of distributed parameter systems, Banff, Alberta, Canada*, volume I.

Wuenning, J. (2007). Small capacity regenerative burners. *Proceedings of the 2007 AFRC-JFRC International Symposium, Advances in Combustion Technology: Improving the Environment and Energy Efficiency, Hawaii, USA*.

Yoshitani, N., Ueyama, T., and Usui, M. (1994). Optimal slab heat-

Post-print version of the article: A. Steinboeck, D. Wild, and A. Kugi, "Nonlinear model predictive control of a continuous slab reheating furnace", *Control Engineering Practice*, vol. 21, no. 4, pp. 495–508, 2013. DOI: 10.1016/j.conengprac.2012.11.012

ing control with temperature trajectory optimization. In *Proceedings of the 20th International Conference on Industrial Electronics, Control and Instrumentation, IECON'94, Bologna, Italy*, volume 3, 1567–1572.

Post-print version of the article: A. Steinboeck, D. Wild, and A. Kugi, "Nonlinear model predictive control of a continuous slab reheating furnace", *Control Engineering Practice*, vol. 21, no. 4, pp. 495–508, 2013. DOI: 10.1016/j.conengprac.2012.11.012
The content of this post-print version is identical to the published paper but without the publisher's final layout or copy editing.